LBL--14644

DE82 018801

Optically Enhanced Nuclear Cross Polarization in Acridine-Doped Fluorene

by

Connie M. Oshiro

Ph.D. Thesis

Chemical Biodynamics Division
Lawrence Berkeley Laboratory
University of California
Berkeley, CA 94720

This work was supported by the Assistant Secretary for Environment, Office of Life Sciences Research and Nuclear Medicine Applications, Division of General Life Sciences of the U.S. Department of Energy under Contract No. DE-AC03-76SF00098.

TABLE OF CONTENTS

1. INTRODUCTION

NMR provides a dynamic and non-destructive probe of the chemical environment. In particular, in a solid or semi-solid where anisotropic interactions such as the chemical shift are retained, many nuclei other than protons can give valuable information about the structure and motion of molecules. However, the NMR signals from nuclei other than protons are extremely weak for a variety of reasons, including:

i) low natural abundance

ii) small gyromagnetic ratio

iii) long spin-lattice relaxation times

iv) in the solid state, the presence of large dipole-dipole interactions and the existence of a quadrapole interaction which may dominate the NMR spectrum and mask chemical shift information.

Various schemes can be used to increase the sensitivity of these other nuclei:

i) use of large magnetic fields

ii) improvement of rf hardware and signal averaging

iii) for the case of dilute spins in solids, use of double resonance techniques, in particular, the proton enchanced nuclear induction spectroscopy (PENIS) experiment, in combination with decoupling techniques.

A combination of the above three schemes is becoming more prevalent in the study of dilute spins in solids. In the PENIS experiment an improvement in signal to noise is accomplished by

transferring the abundant proton polarization to the dilute spins. The intensity of the dilute spin signal is then limited by the polarization of the abundant proton spins.

The objective of this work has been to create large polarizations of the dilute ^{13}C nuclei in the solid state. The idea was to create ^{1}H polarizations larger than Boltzmann and to use the PENIS cross polarization technique to then transfer this large polarization to the ^{13}C spin system.

Optical Nuclear Polarization (ONP) appeared to be an attractive method to create large non-Boltzmann proton polarizations simply and rapidly. Normal Boltzmann polarizations are on the order of .005%. In single crystals of fluorene doped with acridine, proton polarizations on the order of .1% have been reported [1,2]. Such polarizations are equivalent to the sample sitting in a magnetic field of approximately 3 MGauss. Magnetic fields strengths readily avaliable in the laboratory today are aproximately 65 kGauss. The polarization is approximately three orders of magnitude larger than could be conventionally obtained. Additionally, protons in fluorene could be polarized in a time much less than T_1, the spin lattice relaxation time. The ONP polarization time is determined by the illumination time, which is on the order of 1 minute, rather than T_1, which is on the order of 30 minutes.

ONP of acridine-doped fluorene single crystals has been studied here. In addition, ONP of powdered samples of the acridine-doped fluorene has been studied. In general, many compounds do not crystallize easily or do not form large crystals suitable for NMR experiments. Powdered, amorphous and randomly dispersed samples are

generally far more readily avaliable than single crystals. One objective of this work has been to (first) create large ^{1}H polarizations. Although large optical proton polarizations in single crystals have been reported previously [1,2], optically generated polarizations in powdered samples have not been reported. For these reasons, ONP studies of powdered samples of the acridine-doped fluorene were also undertaken.

Using ONP in combination with the PENIS experiment, large ^{13}C polarizations have been created in fluorene single crystals. These large ^{13}C polarizations have permitted the determination of the seven incongruent chemical shielding tensors of the fluorene molecule.

Part 2 of this thesis describes the PENIS experiment. Part 3 describes the ONP experiment. Part 4 is a description of the experimental set-up. Part 5 describes the data analysis for the determination of the chemical shielding tensors. Part 6 presents the results of the ONP experiments performed in this work and the chemical shielding tensors determined.

2. Proton Enhanced Nuclear Induction Spectroscopy

In the proton-enhanced nuclear induction spectroscopy (PENIS) experiment, spin order of an abundant spin species, such as protons, is transferred to a dilute spin system such as ^{13}C, resulting in ^{13}C magnetization greater than Boltzmann. The PENIS experiment has been described by many authors; for example, see Pines, Gibby, Waugh [3] and Mehring [4]. A general description is included here.

2.1 Background

The concept of spin temperature is important for an understanding of the PENIS experiment. It can be stated as follows: a spin system, I, isolated from the lattice and subjected to spin-spin interactions, proceeds toward a state of internal equilibrium such that the population of the spin energy levels is given by an exponential distribution $N(E_i) \propto \exp(-\beta E_i)$. $\beta \approx 1/kTs$ is the inverse spin temperature Ts of the system. If the population distribution is the Boltzmann distribution, Ts is the lattice temperature.

The density matrix ρ of the spin system described by the Hamiltonian H is defined as

$$\rho = \exp(-\beta H)/Tr(\exp(-\beta H)) \qquad 2.1$$

Generally, for T >> 1 degree K, E_i is less than kT for all energy levels of the spin system. Hence ρ can be well approximated by

$$\rho = Z^{-1}[1-\beta H] \qquad 2.2$$

where

$Z = Tr(\underline{1}) = (2I+1)^N$ is the partition function

N is the number of I spins in the sample.

If a large external magnetic field, Ho, is applied to the spin system along the coordinate z axis, the Hamiltonian becomes

$$H = -\gamma h Ho.I = -\gamma h Ho Iz \qquad 2.3$$

where γ is the gyromagnetic ratio of the I spin and h is Planck's constant.

The magnetization and energy of the system are

$$M_i = 1/Z\ h\gamma Tr(\rho I_i) = \beta\ C\ Ho \qquad 2.4$$

$$E = -Tr(\rho H) = -\beta\ C\ Ho^2 \qquad 2.5$$

where

C is the Curie constant equal to $1/3\ N\ I(I+1)\gamma^2h^2$

N is, as stated previously, the number of I spins in the sample.

The term $C\ Ho^2$ is the effective "heat capacity" of the I spins.

Consider a two spin system consisting of an abundant I spin system and a dilute S spin system. Both spins are immersed in a large external magnetic field, Ho. Let the Larmor resonance frequency of the I spins in the field be $\omega_{oI}=h\gamma_I Ho$, and the Larmor resonance frequency of the S spins, $\omega_{oS}=h\gamma_S Ho$. Two strong rf fields of amplitude H_{1I} and H_{1S} are applied at the resonance frequencies ω_{oI} and ω_{oS} of the I and S spin systems. The rf fields are applied in the xy plane perpendicular to the constant field Ho. The full Hamiltonian is

$$H = H_z + H_{dii} + H_{dis} + H_{rf} \qquad 2.6$$

where

H_z is the nuclear Zeeman interaction of both the I and S spins

H_{dii} is the dipolar interactions between I spins

H_{dis} is the dipolar interactions between the I and S spins

H_{rf} is the interaction of the spin system with the rf fields

(scalar couplings have been ignored since $H_{scalar} \ll H_{dii}, H_{dis}$).

For Ho//z

$$H_z = -h\omega_{oI}Iz - h\omega_{oS}Sz$$

$$H_{dii} = \gamma_I^2 \Sigma_{i,j}(I_i \cdot I_j(1-3\cos^2\theta/r^3_{ij}) - 3I_{iz}I_{jz})$$

$$H_{dis} = \gamma_I\gamma_S \Sigma_{i,j}(I_i \cdot S_j(1-3\cos^2\theta/r^3_{ij}) - 3I_{iz}S_{jz})$$

$$H_{rf} = H_{1I}(I_x\cos\omega_{oI}t + I_y\sin\omega_{oI}t) + H_{1S}(S_x\cos\omega_{oS}t + S_y\sin\omega_{oS}t)$$

where

θ_{ij} is the angle between the magnetic field vector and the vector joining the two spins i and j, and

r_{ij} is the distance between the two pairwise coupled spins.

In the doubly rotating frame, the effects of the large magnetic field, Ho, can be eliminated. The operator R which transforms the system from the stationary laboratory frame to this doubly rotating frame is given by

$$R = \exp[-i\omega_I Izt - i\omega_S Szt] \qquad 2.7$$

where ω_I and ω_S are the frequencies of the rotating frames. If $\omega_I = \omega_{oI}$ and $\omega_S = \omega_{oS}$ in this new frame the Hamiltonian becomes

$$H_r = -\gamma_I h H_{1I} Ix - \gamma_S h H_{1S} Sx + H'_{dii} + H'_{dis}$$

$$= H_{II} + H_{IS} + H'_{dii} + H'_{dis} \qquad 2.8$$

This is the Hamiltonian of the PENIS experiment which will be used later in this section.

2.2 Description of PENIS experiment

The PENIS experiment proceeds through 5 major steps:

i) the I spins are polarized

ii) the I spins are cooled

iii) the I and S spins are brought into contact and order transferred from the I spins to the S spins

iv) S spins are detected while decoupled from the I spins

v) parts (iii) and (iv) are repeated until the I spin magnetization is depleted.

In this experiment, the abundant I spins are the protons and the dilute S spins are the ^{13}C in fluorene.

i) polarize I spins

In most cross polarization experiments, the I spins are polarized by placing the sample in a large external magnetic field Ho and waiting a time > T_1, the spin lattice relaxation time. In the experiment described in this thesis, the I spins are polarized optically.

When the I spins are polarized the density matrix of the system is

$$\rho = 1-\beta\ I\ H_z \qquad 2.9$$

Only H_z enters the above equation because $H_z >> H_{dii}$ and $H_{rf}=0$. The

S spins are assumed to be unpolarized at this stage, so that their inverse spin temperature is 0. When the I spins are placed in a large magnetic field Ho and are allowed to equilibrate, the spin temperature defined by the population difference of the abundant spin system equals β_{lat}, the inverse lattice temperature, of the I spin system. The normal Boltzmann magnetization M_{oI} and energy E are

$$M_{oI} = \beta_{lat} C_I Ho \qquad 2.10$$

$$E = -\beta_{lat} C_I Ho^2 \qquad 2.11$$

In the ONP experiment, the I spins are not in thermal equilibrium with the lattice and β_{onp}, the inverse spin temperature of the system, does not equal β_{lat}. An effective magnetic field H' can be defined as that magnetic field which would give rise to the actual I spin polarization at the lattice temperature. The actual magnetization in this case is given by

$$M_I = \beta_{onp} C_I Ho = \beta_{lat} C_I H' = M_{oI} H'/Ho \qquad 2.12$$

In the ONP experiment, $\beta_{onp} >> \beta_{lat}$ and therefore $Ho << H'$.

ii) cool I spins

The I spins can be cooled in a variety of ways. The I spins in these experiments are cooled by spin locking the magnetization (equation [2.12]) along H_{1I} in the rotating frame. (The remaining discussion is limited to this case.) This is accomplished by first applying a 90 degree pulse to rotate the magnetization into the xy plane, followed immediately by a long pulse phase shifted by 90 degrees from the first pulse. The spin locking preserves the original

magnetic ordering along a rotating frame field much smaller than Ho. This results in an effective cooling of the I spins [5].

The Hamiltonian of the system is given by equation [2.8], with $H_{1I} >> H_{dii}, H_{dis}$.

Let the inverse spin temperature of the system at this point be β_i. Neglecting H_{dii}, H_{dis}, the density matrix, magnetization and energy in the rotating frame become

$$\rho_r = Z^{-1}(1 - \beta_i H_{1I}) \qquad 2.13$$

$$M_I = \beta_{onp} C_I Ho = \beta_{lat} C_I H' = \beta_i C_I H_{1I} \qquad 2.14$$

$$\beta_i/\beta_{onp} = Ho/H_{1I} \text{ and } \beta_i/\beta_{lat} = H'/H_{1I} \qquad 2.15$$

$$E = - \beta_i C_I H_{1I}^2 \qquad 2.16$$

iii) bring I and S spins into contact

The S spins are brought into contact with the I spins by applying a second rf field at the S spins resonant frequency. Two cases arise for the amplitude of this rf field:

1) matched Hartman-Hahn condition [6]:

$$\gamma_S H_{1S} = \gamma_I H_{1I} \qquad 2.17(a)$$

i.e., the amplitude H_{1S} of the S spin rf field is chosen such that in the rotating frame, the energy difference of the S spin system is equal to the energy difference of the I spin system

or

2) unmatched Hartman-Hahn condition [3]:

$$\gamma_S H_{1S} = a \gamma_I H_{1I} \text{ , } a>>1 \qquad 2.17(b)$$

Only if the time constant of the energy transfer $T_{IS} < T_{1\rho}$, the rotating frame relaxation time, can the energy exchange be considerable. T_{IS} is a function of the coupling between the I and S spins and the mismatch paramter, a; T_{IS} increases with increasing values of a [3,4,7].

If the Hartman-Hahn condition is satisfied (a=1), rapid energy transfer occurs between the I and S spins since energy conserving mutual spin flips are possible. The heat capacity of the S spins, $C_S H_{1S}^2$ is small and the heat capacity of the I spins, $C_I H_{1I}^2$, large. Energy flows rapidly from the S spin system to the I spin system until a common spin temperature is established. A cooling of the S spins occurs, at the expense of a small heating of the I spins.

If the Hartman-Hahn condition is not satisfied (a>>1), the heat capacity of the S spins is large (since H_{1S} is large) and a large cooling of the S spins occurs, with a concomitant large heating of the I spins. However, T_{IS} can become very long. If T_{IS} exceeds $T_{1\rho}$, effective energy transfer is not possible.

The Hamiltonian, H_r, is given by equation [2.8]. Let the final inverse spin temperature be β_f. The density matrix and energy after the spin temperatures have equalized are given by

$$\rho_f = 1 - \beta_f[H_{1I} + H_{1S}] \qquad 2.18$$

$$E_f = -\beta_f[C_I H_{1I}^2 + C_S H_{1S}^2] \qquad 2.19$$

Assuming conservation of energy, $E_i = E_f$, and $\gamma_S H_{1S} = a\,\gamma_I H_{1I}$

$$\beta_i C_I H_{1I}^2 = \beta_f [C_I H_{1I}^2 + C_S H_{1S}^2] \qquad 2.20$$

or

$$\beta_f/\beta_i = (1 + a^2(\gamma_I^2/\gamma_S^2)\ (C_S/C_I))^{-1}$$

$$= (1 + a^2[N_S S(S+1)]/[N_I I(I+1)])^{-1} \qquad 2.21$$

Let $\epsilon = [N_S S(S+1)]/[N_I I(I+1)]$

Therefore, after one contact,

$$\begin{aligned} M_S &= \beta_f\ C_S\ H_{1S} \\ &= \beta_f\ C_S\ a\ (\gamma_I/\gamma_S)\ H_{1I} \\ &= \beta_i\ C_S\ (\gamma_I/\gamma_S)\ [a/(1+a^2\epsilon)]\ H_{1I} \\ &= \beta_{lat}\ C_S\ (\gamma_I/\gamma_S)\ [a/(1+a^2\epsilon)]\ H' \\ &= (\gamma_I/\gamma_S)\ [a/(1+a^2\epsilon)]\ (H'/H_0)\ M_{0S} \end{aligned} \qquad 2.22$$

M_{0S} is the normal Boltzmann magnetization of the S spins. The gain in magnetization after one contact is thus

$$(\gamma_I/\gamma_S)[a/(1+a^2\epsilon)](H'/Ho). \qquad 2.23(a)$$

For ^{13}C, S = 1/2 and for ^1H, I = 1/2, the gain after a single matched Hartman-Hahn contact ($\epsilon \ll 1$, a=1, $[a/(1+a^2\epsilon)] = 1$) is

$$(\gamma_I/\gamma_S)\ (H'/Ho) = 4\ (H'/Ho). \qquad 2.23(b)$$

Under unmatched Hartman-Hahn conditions, the magnetization, M_S, is maximal when $a=(\epsilon)^{-1/2}$ and the gain after a single shot is

$$1/2\ (\gamma_I/\gamma_S)\ (\epsilon)^{-1/2}\ H'/Ho = 1/2(\gamma_I/\gamma_S)\ (N_I/N_S)^{1/2}\ (H'/Ho) \qquad 2.24(a)$$

For ^{13}C at natural abundance, $(N_I/N_S)=200$ and equation 2.24a

becomes

$$\approx 30\ (H'/Ho). \qquad 2.24(b)$$

iv) detect S spins

The H_{1S} field is turned off suddenly and the proton enhanced free induction decay of the S spins is detected and recorded in the presence of the H_{1I} proton field. The H_{1I} field now acts as a decoupling field effectively removing the ^{13}C-^{1}H dipolar interaction by modulating the flip-flop rate of the I spins. For a more detailed account of decoupling, see descriptions by Mehring [4] and Abragham [8].

v) recontact

If the proton reservoir is not depleted, a second (or a third, etc.) contact can be made and the ^{13}C signal(s) added. This is possible when $T_{IS} \ll T_{1\rho}$ with the matched Hartman-Hahn condition, but generally not possible with the unmatched Hartman-Hahn condition.

With multiple contacts and the Hartman-Hahn condition satisfied, the S magnetization after the kth contact is given by

$$M^{k}_{S}=(\gamma_I/\gamma_S)\ (H'/Ho)\ [1/(1+\varepsilon)]^{k}\ M_{oS} \qquad 2.25$$

Therefore, the final magnetization is given by,

$$\begin{aligned} M_S &= (\gamma_I/\gamma_S)\ (H'/Ho)\ M_{oS}\ \Sigma_{k=1,n}[1/(1+\varepsilon)]^{k} \\ &\approx (\gamma_I/\gamma_S)\ (H'/Ho)\ M_{oS}\ \Sigma_{k=1,n}(1-\varepsilon)^{k} \end{aligned} \qquad 2.26$$

If n contacts are done and the signals co-added, and assuming $n\varepsilon \approx 1$,

$$\Sigma_{k=1,n}(1-\epsilon)^k \approx 1/2\epsilon \qquad 2.28$$

The gain (in signal to noise) at the end of the nth contact (again, with $n\epsilon \approx 1$) is

$$1/2\ (\gamma_I/\gamma_S)(n)^{-1/2}(1/\epsilon)H'/Ho \approx 1/2\ (\gamma_I/\gamma_S)(N_I/N_S)^{1/2}(H'/Ho) \qquad 2.29$$

That is, the gain at the end of a multiple contact, matched Hartman-Hahn PENIS experiment is approximately equal to the gain of a one shot, unmatched Hartman-Hahn PENIS experiment.

Ideally, large ^{13}C polarizations (on the order 30 H'/Ho) can be obtained using either multiple contact matched Hartman-Hahn conditions or one-shot, unmatched Hartman-Hahn conditions. The acridine-doped fluorene system is ideally suited for either case: $T_{1\rho}$ is very long [47], on the order of a second. Approximately 1/2 of the total I-proton spin polarization can, in theory, be transferred to the S-carbon spins. For practical reasons (e.g.,to avoid probe burn-out), a one-contact, matched Hartman-Hahn experiment was perfomed here. The gain in this case is (only) 4 H'/Ho; the dominant term for gain, H'/Ho. Large S-carbon polarization can still be obtained by making $H'/Ho \gg 1$. This was accomplished by first optically polarizing the protons (see next section). It follows, however, with $H'/Ho \gg 1$, that the gain for a multiple contact or a one-shot unmatched Hartman-Hahn experiment would be far larger.

3. Optical Nuclear Polarization

Optical Nuclear Polarization (ONP) is the non-Boltzmann proton polarization created by illuminating the sample with light. ONP can be created via different mechanisms in different systems. The mechanism particular to the acridine-doped fluorene system is described here. Descriptions of this mechanism can be also be found in papers by Stehlik, Hausser, et al [1,9,10] and by V. Macho in his thesis [11].

The essential ingredients for ONP are:

i) an optically induced non-Boltzmann population of the excited electronic triplet state of the system

ii) a static electron-nuclear hyperfine interaction, which creates eigenstates which are mixtures of the electronic and nuclear basis states of the system

iii) a selective electronic decay scheme which produces different decay rates from the various excited triplet substates to the ground singlet substates of the system.

ONP occurs when the return rates from the excited triplet substates to the proton Zeeman ground α and β states differ (α=eigenstate parallel to magnetic field; β=eigenstate anti-parallel to magnetic field).

The ONP effect can be understood by considering a single proton nuclear spin, I=1/2, 2 electron, S=1, system. In a solid all the proton nuclear spins are tightly coupled and rapidly come to the same spin temperature. The only measurable quantity is the polarization of the total nuclear spin reservoir which can be described by considering

simply 1 proton. The simple 1 proton, 2 electron system considered here consists of the ground and excited electronic singlet (So and S_1 respectively) and triplet (Tx,Ty,Tz) states, each broken into doublets with the inclusion of the nuclear spin substates (α,β). Figure 3.1 depicts the relevant transitions for this system in a Jablonski energy level diagram.

A more detailed description of the ONP effect follows. Part 1 describes the various rate equations which govern the growth of optical nuclear polarization; part 2 determines the population and decay rates of the various sublevels of the system which enter into the ONP rate equations; part 3 briefly disusses the selective population and decay rates of the excited triplet state; part 4 discusses the mixing coefficients which are used to determine the population and decay rates of part 2; part 5 briefly discusses the level anti-crossing phenomenon which is responsible to the large non-Boltzmann proton polarizations in acridine-doped fluorene single crystals.

3.1 Rate equations

For a nuclear spin I=1/2 in a magnetic field Ho, the nuclear polarization is defined as

$$p = (n_\alpha - n_\beta)/(n_\alpha + n_\beta) \qquad 3.1$$

where n_λ is the population of the λth nuclear sublevel of the electronic ground state ($\lambda = \alpha$ or β) The population n_λ is governed by the rate equation,

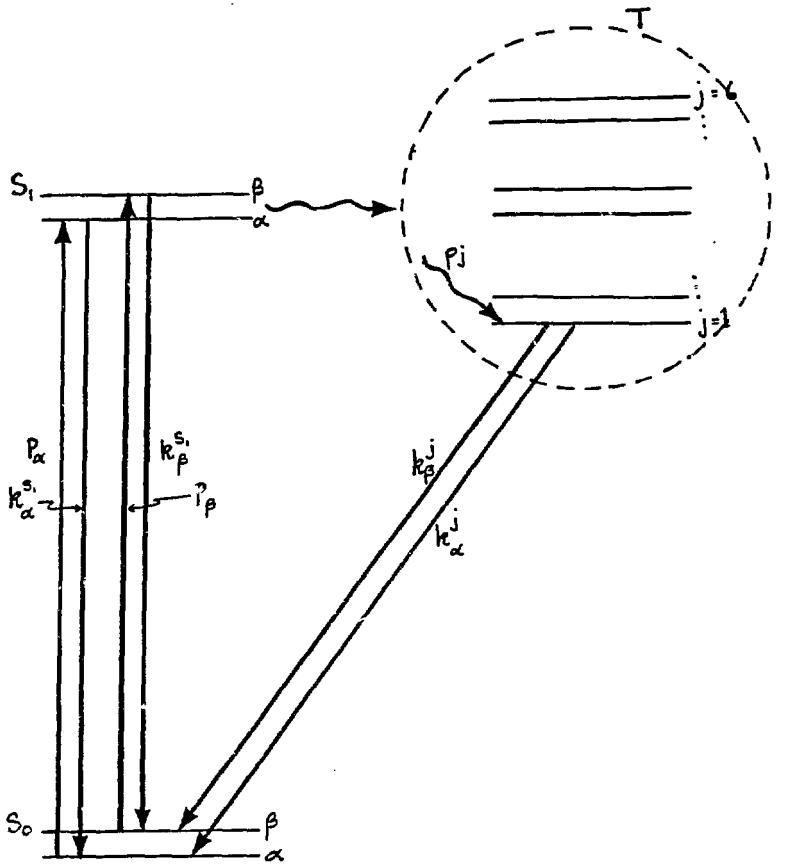

Figure 3.1 Jablonski energy level diagram with relevant transitions. Energy level splittings not drawn to scale.

$$dn_\lambda/dt = -P_\lambda n_\lambda + k^{S1}{}_\lambda N_{S1} + \Sigma_j k^j{}_\lambda N_j \qquad 3.2$$

where (see figure 3.1)

P_λ is the optical pump rate out of nuclear sublevel λ of the ground state

$k^{S1}{}_\lambda$ is the decay rate out of the S1 λ excited state to the sublevel λ of the ground state

$k^j{}_\lambda$ is the decay rate out of the jth excited triplet state to sublevel λ of the ground state

N_j is the population of the jth excited triplet state

Here and in later discussions, Greek letters refer to the nuclear spin states and the label j to an excited triplet eigenstate sublevel.

Since the transitions into and out of the ground singlet and the exited singlet states are electronic dipole transitions, the nuclear quantum number λ is conserved and the pump rates P_λ and decay rates $k^j{}_\lambda$ are independent of nuclear sublevel λ--

$$P_\alpha = P_\beta \qquad 3.3$$

$$k^{S1}{}_\alpha = k^{S1}{}_\beta \qquad 3.4$$

Assuming the nuclear spins are initially unpolarized, the final nuclear polarization is determined by the polarization created per triplet state and the number of triplet states. The polarization growth rate is governed by the rate equation

$$dp/dt = d(n_\alpha - n_\beta)/dt = \Sigma_j (k^j{}_\alpha - k^j{}_\beta) N_j \qquad 3.5$$

From eqn [3.5] it can be seen that if $k^j{}_\alpha$ is not equal to $k^j{}_\beta$ for

each of the jth triplet levels, a nuclear polarization can develop.

The relative populations N_j of the triplet sublevels are governed by the rate equations,

$$dN_j/dt=\Sigma_\lambda P^\lambda{}_j n^{S1}{}_\lambda-(k^j{}_\alpha+k^j{}_\beta)N_j-\Sigma w_{ij}[(N_i-N_j)-(N_{i0}-N_{j0})] \qquad 3.6(a)$$

where

$P^\lambda{}_j$ is the populating rate from the S_1 λth excited state

$n^{S1}{}_\lambda$ is the population of the S_1 λth excited state

w_{ij}, the spin lattice relaxation rate, is the transition rate from triplet level i to triplet level j

N_{j0} is the Boltzmann population of the triplet level.

For a single created triplet state,

$$\Sigma_\lambda P^\lambda{}_j n^{S1}{}_\lambda \simeq P_j(n^{S1}{}_\alpha + n^{S1}{}_\beta) = P_j \qquad 3.6(b)$$

and equation 3.6a becomes

$$dN_j/dt = P_j-(k^j{}_\alpha+k^j{}_\beta)N_j-\Sigma w_{ij}[(N_i-N_j)-(N_{i0}-N_{j0})] \qquad 3.6(c)$$

Assuming the optical system is in a steady state, $dN_j/dt = 0$, and a large increase in the populations of all the triplet states ($N_j \gg N_{j0}$), the solution to the population equation 3.6c is

$$P_j = (k^j{}_\alpha+k^j{}_\beta)N_j + \Sigma w_{ij}[N_i-N_j] \qquad 3.7$$

which gives N_j as an implicit function of P_j and w_{ij}. The problem then reduces to determing the rate constants $k^j{}_\lambda$, P_j and w_{ij}.

3.2 Population and decay rates N_js, $k^j{}_\lambda$s

The transitions from the excited triplet to the ground singlet

are strictly electronic transitions. In the absence of hyperfine interaction, the electronic triplet sublevels would be simply direct products of the electronic and the nuclear basis states (in the zero field basis states, they could be represented as $[Tx,Ty,Tz,] \otimes [\alpha,\beta]$). Since the decays from the triplet state to the ground state are electronic transitions, independent of nuclear quantum number, $k^j_\alpha = k^j_\beta$ for all triplet substates j when the eigenstates are products of the pure states; nuclear polarization does not develop. However, the electron-nuclear hypefine interaction mixes the pure triplet sublevels leading to eigenstates which are linear combinations of the pure $T_l, l=x,y,z$. The admixture of the other states, parametarized by the mixing coefficients, $c^j_{l\lambda}$, leads to the inequality $k^j_\alpha \neq k^j_\beta$ and allows ONP to develop.

The total Hamiltonian of the combined electron triplet, S=1, and nuclear spin system, I=1/2, in an external magnetic field Ho is given by

$$H = H_e + H_n + H_{hf} \qquad 3.8$$

where

$$H_e = H_{zero} + H_{zeeman}$$
$$= S.D_e.S + bHo.g.S$$
$$= D(S_z^2 - 1/3\ S^2) + E(S_x^2 - S_y^2) + bHo.g.S$$

in the principal axis system of the tensor De

$$H_n = \gamma_n h\ Ho.I$$
$$H_{hf} = h\ I.A.S$$

H_{zero} is the dipole-dipole interaction between the 2 unpaired

electron spins S_1 and S_2 which make up the triplet state; $S = S_1+S_2$.
De is the dipolar interaction tensor;
H_{zeeman} is the electron-magnetic field interaction
H_n is the nuclear spin-magnetic field coupling;
H_{hf} is the coupling between the electron and the nuclear spin; A denotes the hyperfine coupling tensor. The orientation of the hyperfine tensor A need not be coincident with the zero field tensor. In this system, A is not coincident with the dipolar tensor D_e [12].

The Hamiltonian is represented in matrix form in figure 3.2, with the zero field triplet states as the basis states. p, q, and r represent the direction cosines of the magnetic field with respect to the triplet axes defined by the orientation of the electron dipolar tensor D_e. The six eigenstates of the system are determined by diagonalizing this Hamiltonian.

3.2.1 Determination of k's

After diagnolizing the Hamiltonian, let the eigenstates $|j\rangle$ be given by

$$|j\rangle = \Sigma\, c^{j}_{l,\lambda}\, |T_l\ \lambda\rangle \qquad l=x,y,z \quad \lambda=\alpha,\beta \tag{3.10}$$

where the $c^{j}_{l,\lambda}$ are the mixing coefficients.

If V is the coupling causing the transitions from the excited triplet states to the ground state So,

$$\begin{aligned} k^{j}_{\lambda} &= |\langle So\,|\,V\,|\,j\rangle|^2 \\ &= |\langle So\,|\,V\,|\,\Sigma\, c^{j}_{l,\lambda}\ T_l\ \lambda\rangle\ ^2 \\ &= \Sigma\left|c^{j}_{l,\lambda}\right|^2 |\langle So\,|\,V\,|\,T_l\rangle|^2 \end{aligned} \tag{3.11}$$

$T_{x\alpha}$	$T_{y\alpha}$	$T_{z\alpha}$	$T_{x\beta}$	$T_{y\beta}$	$T_{z\beta}$
$D-E-1/2\ g_n\beta_n rH$	$-i(1/2\ A_{zz}+g_{zz}\beta_e rH)$	$i(g_{yy}\beta_e qH+1/2\ A_{yz})$	$-1/2\ g_n\beta_n(p-iq)H$	$-1/2\ A_{yz}$	$1/2\ A_{yy}$
	$D+E-1/2\ g_n\beta_n rH$	$-ig_{xx}\beta_e pH$	$1/2\ A_{yz}$	$-1/2\ g_n\beta_n(p-iq)H$	$-1/2\ A_{xx}$
		$-1/2\ g_n\beta_n rH$	$-1/2\ A_{yy}$	$i/2\ A_{xx}$	$-1/2\ g_n\beta_n(p-iq)H$
			$D-E+1/2\ g_n\beta_n rH$	$i(1/2\ A_{zz}-g_{zz}\beta_e rH)$	$i(g_{yy}\beta_e qH-1/2\ Ayz)$
				$D+E+1/2\ g_n\beta_n rH$	$-ig_{xx}\beta_e pH$
					$1/2\ g_n\beta_n rH$

Figure 3.2 ONP spin Hamiltonian. The lower triangular part of the matrix can be found by the relation $H_{ij}' = H_{ji}$. See text for details.

All dependence on nuclear quantum number λ is contained in the mixing coefficients $c^j_{l,\lambda}$. The factor $|\langle So | V | T_l \rangle|^2$ depends only on the electron quantum number, l=x,y,z and can be measured by optically detected magnetic resonance and/or estimated if not known.

3.2.2 Determination N_j's

The population N_j is determined by equation [3.7], reproduced here for convenience.

$$P_j = (k^j_\alpha + k^j_\beta)N_j + \Sigma w_{ij}[N_i - N_j] \qquad 3.7$$

If Vo represents some intersystem crossing operator between the excited singlet state S_1 and the triplet state T_l,

$$\begin{aligned} Pj &= |\langle j | Vo | S_1 \rangle|^2 \\ &= |\langle \Sigma c^j_{l,\lambda} T_l \lambda | Vo | S_1 \rangle|^2 \\ &= \Sigma_{l\lambda} |c^j_{l,\lambda}|^2 |\langle T_l | Vo | S_1 \rangle|^2 \end{aligned} \qquad 3.12$$

Again, the factor $|\langle T_l | Vo | S_1 \rangle|^2$ depends only upon the electron quantum number and all the dependence on the nuclear quantum number, λ, is contained in the mixing coefficients, $c^j_{l,\lambda}$.

The w_{ij}'s, the triplet spin lattice relaxation rates can be determined as sums of the T_l-dependent matrix elements times λ-dependent mixing coefficients in a manner analogous to the method used to the determine k^j_λ and p_j.

Given w_{ij}'s, p_j's, k^j_λ eqn 3.7 can then be solved for N_j. In matrix notation,

$$P = (K+W)N \text{ or}$$

$$N = (K+W)^{-1}P \qquad 3.13$$

where

W is the 6X6 symmetric matrix with elements $w_{ii} = 0$, $w_{ij} = w_{ji}$

K is the diagonal 6x6 matrix with elements $k_{jj}=k^j{}_\alpha+k^j{}_\beta$ and $k_{ij}=0$

P is the 6x1 matrix with elements p_j.

3.3 Selective rates

The total wave function of the electron, Ψ, consists of an orbital part, Φ and a spin part, S or T_1 (the orbital wave function has been dropped in the discussion above). That is,

$$\Psi_S = \Phi_S S \qquad \Psi_{T1} = \Phi_{T1}\, T_1,\ 1=x,y,z \qquad 3.14$$

The factor $|\langle\Psi_S | V| \Psi_{T1}\rangle|^2$ (called $|\langle S | V| T_1\rangle|^2$ above) can be measured and/or estimated.

V is, oftentimes, the spin-orbit coupling operator; it is the interaction of the magnetic moment of the spinning electron with the magnetic field produced by the relative motion of the electrons and nuclei. Exact evaluation of the matrix element is complex, but for molecules having C_{2v} symmetry, or higher, predictions for non-vanishing matrix elements can be made using purely group theoretical agruments. For descriptions of symmetry selection rules and group theory, see, for example, Tinkham [13] and van der Waals and de Groot [14].

All molecular wave functions belong to one of the irreducible representations, Γ, of the molecular symmetry group. From group theory, $|\langle\Psi_S | V | \Psi_{T1}\rangle|^2 \neq 0$ only when the function being integrated is

symmetric, i.e., the direct product of the representations of ψ_S, V, and ψ_{T1} contains the totally symmetric irreducible representation, A.

$$A \in \Gamma_{\psi S} \otimes \Gamma_V \otimes \Gamma_{T1} \qquad 3.15$$

$\Gamma_{V=\text{spin orbit}} \in A$ and $\Gamma_{\phi S} \in A$, from the "great orthogonality theorem" [13] equation [3.15] reduces to

$$\Gamma_{\phi S} = \Gamma_{\phi T1} \otimes \Gamma_{T1} \qquad 3.16$$

With C_{2v} symmetry, T_1 1=x,y,z each belongs to different (orthogonal) irreducible representations. Therefore, $|\langle\psi_S | V | \psi_{T1}\rangle|^2$ will be non-zero for no more than one value of 1. Selective population in to and decay out of the triplet state can therefore occur.

3.4 Mixing coefficients

The ONP signal can be very large when the mixing coefficients are very large. The mixing coefficients are determined exactly by diagonalizing the Hamiltonian, but this gives little insight into their behavior as a function of the applied magnetic field Ho.

From first order perturbation theory, the eigenstate j is given by

$$|j\rangle = T_1{}^{\lambda} + \Sigma_{1'\lambda'} c^{j}_{1'\lambda',T_1,\lambda'} \qquad 3.17$$

The mixing coefficients are given by

$$c^{j}_{1'\lambda'} = \frac{\langle T_{1'}{}^{\lambda'} | \mathcal{H} | T_1{}^{\lambda}\rangle}{E_{1\lambda} - E_{1'\lambda'}} \qquad 3.18$$

$\langle T_{1'}{}^{\lambda'} | \mathcal{H} | T_1{}^{\lambda} \rangle$ are the off-diagonal elements of the Hamiltonian matrix in figure 3.2. The mixing coefficients will be large when either the hyperfine interaction A is large, or when the energy separation between the strictly electronic basis states, δE, is small.

3.5 Level Anti-crossing

δE is small when two of the triplet energy levels appear to cross each other. When these levels are coupled by some perturbing interaction, they will mix and the new eigenstates of the system are linear combinations of the orignal states. This phenomenon is known as level anti-crossing. For a more extensive treatment of level anti-crossing, see Stehlik [10] and Veeman [15,16].

From the Hamiltonian in equation 3.9, it can be seen that the eigenstates of the system depend upon the strength and orientation of the applied magnetic field Ho with respect to the triplet axes. Figures 3.3 and 3.4 illustrate the field dependence of the energy levels of H_e when Ho//y and Ho//z. Points labelled Hy_{1a} and Hz_{1a} are points of level anti-crossings. The top diagram in each figure illustrates the energy levels without the level anti-crossing phenomena. The new states are seen in the lower diagrams.

Figure 3.5 contains theoretical plots of the ONP as a function of field strength when the magnetic field is oriented along one of the zero field principal axes. The mixing coefficients, $c^j_{1\lambda}$'s, are large at Hy_{1a} and Hz_{1a}. A characteristic dispersion-like curve due to level anti-crossing is observed when H//z at approximately 140 gauss. Large ONP signals are observed when the magnetic field is oriented along the y axis in a field of approximately 80 gauss, near the level anti-

crossing region.

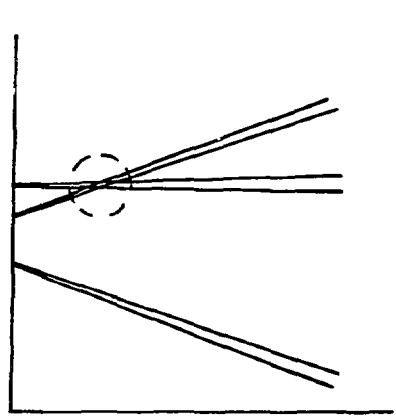

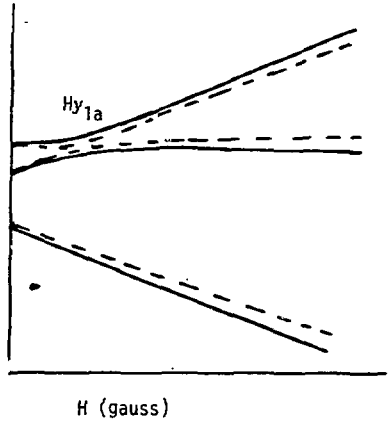

Figure 3.3 Triplet energy levels, H//y. Top diagram: level-crossing. Bottom Diagram: level anti-crossing.

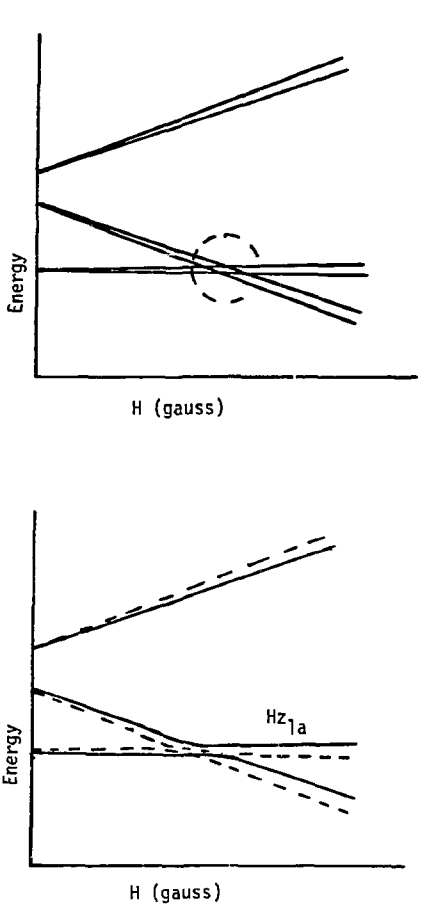

Figure 3.4 Triplet energy levels, H//z. Top diagram: level-crossing. Bottom diagram: level anti-crossing.

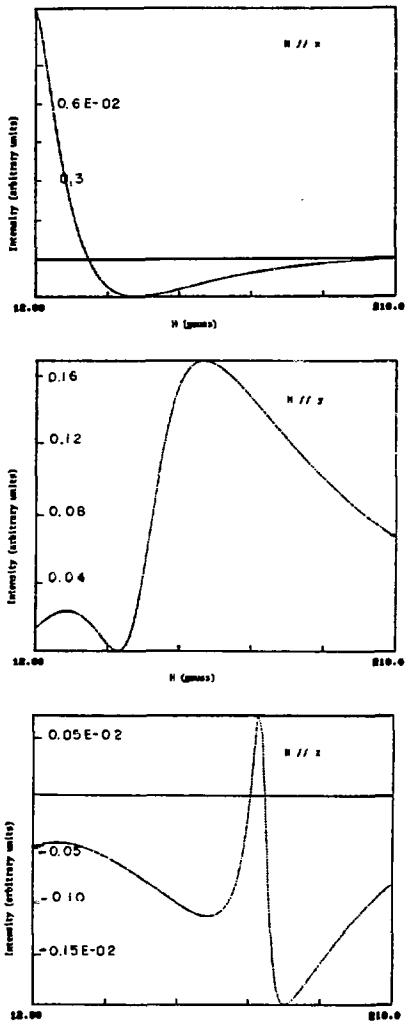

Figure 3.5 Computed proton ONP as a function of Hp oriented along a principal axis. The horizontal line denotes a polarization equal to the Boltzmann signal.

4. EXPERIMENTAL SET-UP

All experiments were done using a two field technique. An initially unpolarized crystal was fixed in orientation in a polarizing field Hp of preset amplitude. The crystal was irradiated by broad-band unpolarized uv light for a time Δt, after which the light was turned off. The crystal was then adiabadically moved to a measuring field Hm and either i) the optically generated proton polarization was measured, or ii) the ^{13}C spins were cross polarized and the ^{13}C spectrum was measured.

Figure 4.1 and 4.2 contain a diagram of the experimental setup. The experimental apparatus consisted of

i) the polarizing magnetic field

ii) the optical system and

iii) a home-built double resonance spectrometer.

In order to create a larger working area above the probe, the 14 kGauss Varian magnet which provided the measuring field was rotated 45 degrees, as described by Kohler [17] and shown in figure 4.1. The optical setup was placed above the Varian magnet. The sample could be moved smoothly in and out of both the polarizing field and the measuring field.

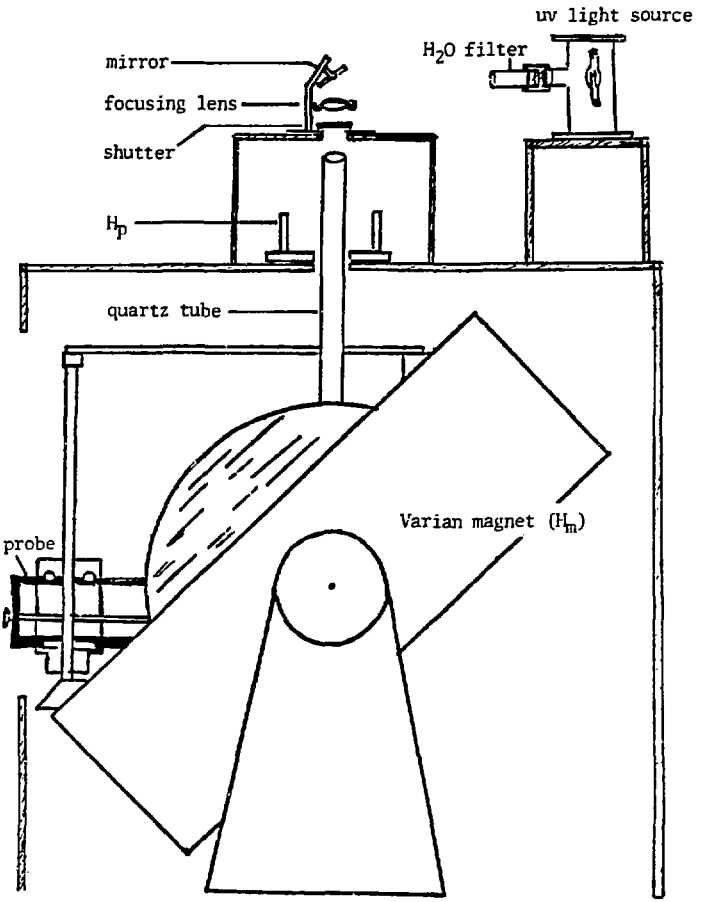

Figure 4.1 Experimental set-up: physical layout two field technique.

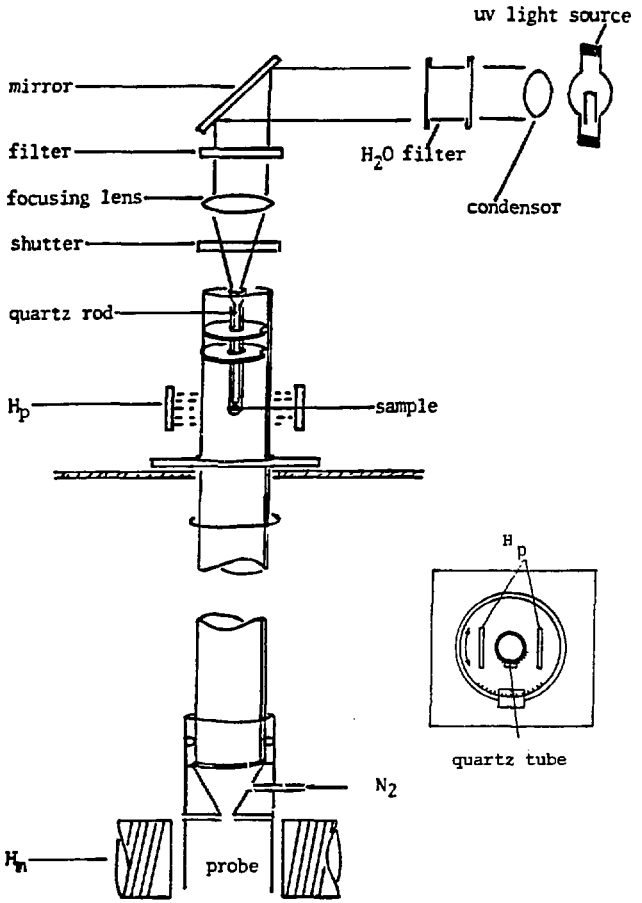

Figure 4.2 Optical set-up.

4.1 polarizing field

4.1.1 ONP

In general, in the ONP experiments, the polarizing field Hp was the residual magnetic field present at various heights above the center of the 14.1 kGauss fixed field Varian magnet which provided the measuring field. The strength of the residual field was measured at various points using a Bell 811A gaussmeter. The residual field appeared to be parallel to the measuring field Hm. A list of field strength vs. distance from the center of the magnet is shown in Table 4.1.

The crystal was mounted at the bottom of the NMR tube. The NMR tube and the NMR tube holder were contained in a larger quartz tube which was mounted above the probe in the center of the magnet.

The crystal was positioned at various points along the quartz tube, depending upon the polarizing field which was needed, by means of a controlled flow of N_2 through the quartz tube. When the N_2 was turned on, the NMR tube holder and tube containing the crystal would rise as far as a stopper positioned to place the crystal at the chosen polarizing field. When the N_2 was turned off, the crystal would drop into the center of the magnet and into the probe. The NMR tube holder was grooved to fit into a guide in the quartz tube which prevented the NMR tube from rotating within the quartz tube. The quartz tube could be rotated about an axis perpendicular to both Hp and Hm to change the orientation of the crystal with respect to Hp and Hm.

The orientation of the crystal with respect to the magnetic

fields was determined by noting the angle the guide of the quartz tube made with a fixed circle marked in polar coordinates mounted above the center of the magnet.

4.3.2 PENIS experiments

In the ^{13}C experiments, the polarizing field Hp was produced by a pair of small magnetic plates held 10.5 cm apart to give a field strength of 80 gauss in the gap between them. The magnetic plates were positioned high above the center of the magnet. The residual field was <5 gauss. Its effects could essentially be ignored. Hp and the orientation of the crystal with respect to Hp were chosen to produce the maximum ONP.

As in the ONP experiments, the quartz tube containing the crystal in the NMR tube could be rotated to change the orientation of the crystal with respect to the measuring field Hm. The 80 gauss field Hp could also be rotated to keep constant the orientation of the polarizing field with respect to the crystal. In this way the maximum ONP could always be generated.

Table 4.1

Distance from center of magnet (cm)	H_p (gauss)
12	4000
13	3400
14	2900
15	2520
16	2150
17	1900
18	1600
19	1300
20	1180
21	1050
22	940
23	820
24	715
25	615
26	530
27	460
28	390
29	330
30	290
31	250
32	210
33	180
34	150

Table 4.1 (continued)

Distance from center of magnet (cm)	H_p (gauss)
35	130
36	110
37	95
38	80
39	65
40	55
41	45

4.2 optical system

The samples were illuminated with an Osram 1000 watt Hg-Xe lamp contained in a C-60-50 Oriel housing and powered by a Schoeffel power supply LPS 255HR. The housing contained a 2" condensor to collimate the light. IR wavelengths were filtered out with a 2" continuous flow water filter, Oriel #6123. Since fluorene absorbs at wavelengths shorter than 300 nm, acridine, the guest molecule in the crystal, was selectively excited by using a Corning band pass 1-64 filter which cut off wavelengths < 320 nm. The filter was necessary to prevent decomposition of the crystal. Illumination without the filter caused a "burning" of the top layer of the crystal and significant signal loss after an hour of continuous illumination.

The uv light was focussed with a 5 cm diameter 15 cm focal length quartz lens onto the top of a quartz rod, which acted as a light pipe. The rod was held in place in the NMR tube and positioned with the end < 1mm from the crystal. The top of the rod was flared with a cone angle of 20 degrees such that the diameter of the rod at the top of the cone was 1-1/2 times the diameter of the rest of the rod. The NMR tube and quartz rod were moved as a unit in and out of the polarizing and measuring fields.

Light and dark cycles were controlled by a shutter operating in the bulb mode. The shutter release was attached to a solenoid which was controlled by gating an attached ac switching relay.

4.3 spectrometer

All NMR measurements were done on a homebuilt spectrometer built around a 14.1 kGauss Varian electro-magnet. The ^{13}C Larmor frequency in this field was 15.1 MHz; the ^{1}H Larmor frequency was 60 MHz. The NMR spectrometer consisted of

i) the probe circuit

ii) the associated rf hardware which generated the rf transmitter pulses and detected the signal

iii) the transient recorder and signal averager/computer

iv) the lock channel.

Figure 4.3 and 4.4 contain a block diagram of the spectrometer including the probe and the associated rf hardware for the ONP and PENIS experiments.

4.3.1 probe

Various probe designs were considered [18]. The final probe circuit was a double-tuned resonance circuit based on a design by Waugh and co-workers [19]. The probe circuit diagram is shown in figure 4.5, along with the two equivalent resonance circuits which compose the probe. The associated $\lambda/4$ cables which protect the preamplifiers and the $\lambda/2$ cables which block the signal from the transmitter amplifiers are also shown.

The coil was tuned to the two Larmor resonant frequencies of ^{13}C and ^{1}H necessary for the PENIS experiment. The two tuned circuits were isolated by 35 dB by use of the $\lambda/4$ @ 60 MHz cables. In the PENIS experiments, the single coil was used to transmit the rf fields for ^{13}C and ^{1}H (transmitter mode) and used to detect the ^{13}C signals

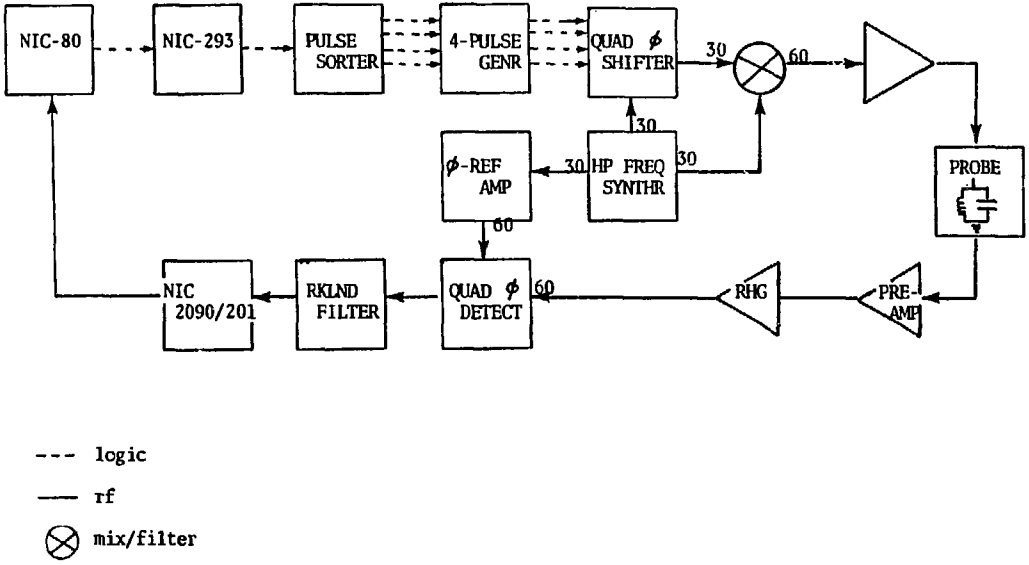

Figure 4.3 Block diagram ONP experiment.

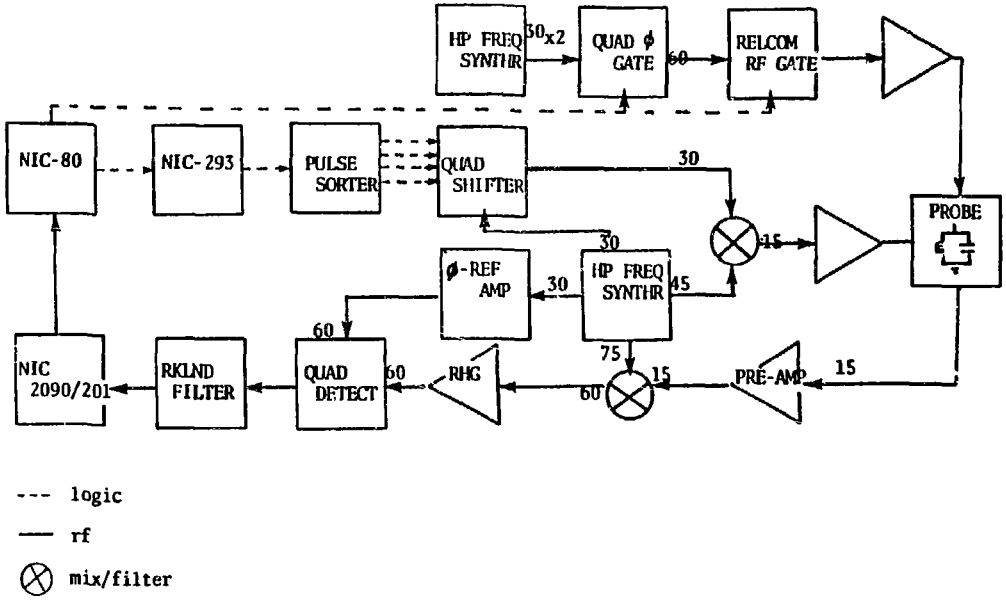

Figure 4.4 Block diagram PENIS experiment.

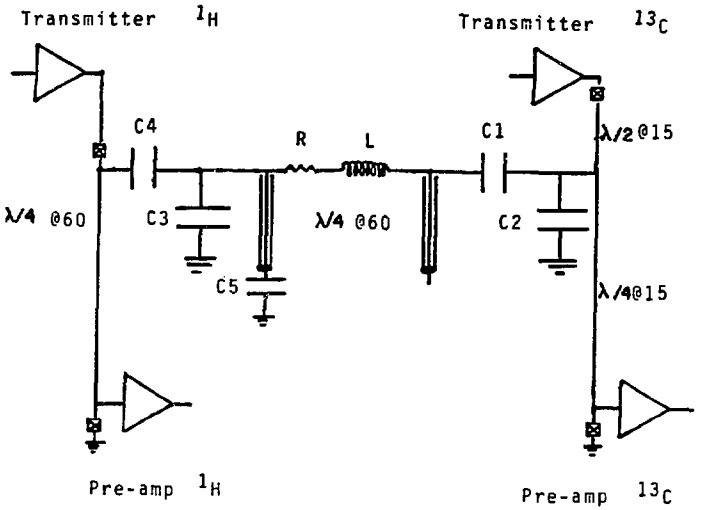

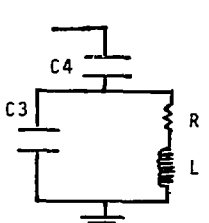

^{1}H 60 Mhz

equivalent circuit

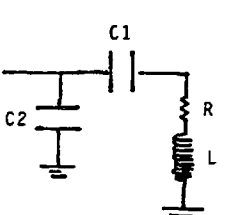

^{13}C 15 Mhz

equivalent circuit

Figure 4.5 Probe circuit.

(receive mode). In the ONP experiments, only the ^{1}H resonant circuit was used; it provided the necessary transmitter pulses and detection of the signal.

The double tuned coil configuration was chosen for two reasons:

i) to save space in the probe

ii) to allow effective power transfer and signal detection for both ONP (proton) and PENIS (carbon) experiments.

The probe Q @ 15 MHz was 30. The ^{13}C field produced by the coil was 48 gauss with 500 watts of power. The ^{1}H field was 12 gauss with 50 watts.

The coil was a 1.5 cm long, 12 turn solenoid made from flattened 20 gauge copper wire with an inductance of 0.15 μh. R in figure 4.5 was a 1 watt, 0.27 ohm resistor which acted as a fuse to protect the coil and capacitors from burning out if too much power was accidentally sent to the probe.

The ^{13}C side of the probe circuit consisted of fixed ATC ceramic capacitors C1 and C2, the coil L and the shorted $\lambda/4$ @ 60 MHz cable. C1 tuned the coil to 15.1 MHz; C2 impedance-matched the tuned resonant ciruit to the 50 ohm impedance of the rest of the system. The shorted $\lambda/4$ @ 60 MHz provided the return to ground for the 15 MHz side. To compensate for the large inductance of the shorted $\lambda/4$ @ 60 MHz cable at 15.1 MHz large value capacitors were added before the return to ground.

The ^{1}H side of the probe circuit consisted of capacitors C3 and C4, the coil, L, and the open $\lambda/4$ @ 60 MHz cable. The capacitors were 0.8-10 pf Johanson 5761 variable capacitors in parallel with fixed ATC ceramic capacitors. C3 tuned the coil to 60 MHz; C4 impedance

matched the proton resonant circuit to 50 ohms. The open λ/4 @ 60 MHz cable provided an effective ground. The effects of the shorted λ/4 @ 60 MHz could essentially be ignored.

4.3.2 Associated rf hardware

4.3.2.1 PENIS

^{13}C:transmit

To create the necessary 15.1 MHz rf field of the correct phase, a fixed frequency phase-shifted 30 MHz signal was mixed with a 45.1 MHz signal.

HP 5100A frequency synthesizer provided both the 45.1 MHz and the fixed 30 MHz. The 30 MHz went immediately to the quadripolar phase splitter (LBL 16x627) which was gated to put out the appropriate sequence of the four quardrature phases, (0,90,180,270). The transmitter rf phases followed the standard 4 pulse Stejskal-Schaefer, add/subtract quadrature phase sequence [20]. The selected output phase was mixed with the 45.1 MHz with an HP 10514A mixer, then low pass filtered through a 30 MHz low pass Cir-q-tel filter 20-30-9/50 to form 15.1 MHz of the correct phase. This was then amplified by a Bruker high power amplifier then sent to the probe.

^{13}C:receive

The signal from the probe was fed through a low noise preamplifier designed by W.C.Shih [21]. A series of shorted λ/4 @ 15 MHz cables preceeded the the preamplifier to protect it from rf transmitter pulses. A Cir-q-tel 30 MHz low pass filter formed part of the λ/4 line to prevent 60 MHz from saturating the 15.1 MHz preamplifier.

The detection system was based on an intermediate frequency of 60 MHz. The 45.1 MHz and the 30 MHz from the frequency synthesizer were mixed to form 75.1 MHz. This 75.1 MHz was filtered and amplified then combined with the output of the preamplifier to form 60 MHz. The 60 MHz was then amplified by an RHG amplifier (LBL 10x1550), then sent to the quadrature phase detector (LBL 10x19550). The dc outputs of the quadrature phase detector were filtered through Rockland 442 filter, recorded on a Nicolet 2090/201 transient recorder, then transferred to and signal averaged on a Nicolet-80 computer. Raw data were transferred to the VAX/VMS 11/780 for archival storage. Fourier transformed data were transferred to the VAX for plotting and analysis.

^{1}H:transmit

The 60 MHz Larmor frequency of the protons was generated by doubling the appropriate value 30 MHz output of a second HP frequency synthesizer 5100B. The 60 MHz was sent to a gated phase shifter, then to a Relcom rf switch. The resulting rf pulses were then amplified through a series of amplifiers: a homebuilt 60 MHz amplifier (LBL 16x970) which contained a Watkins-Johnson A-7 and a Motorola 592, followed by a KLM amplifier and a Henry radio amplifier both tuned to 60 MHz.

4.3.2.2 ONP

As in the PENIS experiment, 60 MHz was generated by doubling 30 MHz.

The 30 MHz output of the HP frequency synthesizer was split 3 ways. One output went to the quadrature phase splitter which again

provided the correct sequence of quadrature phases. The output of the splitter was combined with the second 30 MHz output of the synthesizer to form the proton Larmor 60 MHz of the correct phase. This was then amplified by the same series of amplifiers as in the PENIS experiment.

The detection system was based on an intermediate frequency of 60 MHz. The third 30 MHz output of the synthesizer was doubled and used as the reference frequency in the receiver system.

The output of the probe was sent to a low noise preamplifier designed by B.Leskovar [22]. The preamplifier was preceeded by a series of shorted $\lambda/4$ @ 60 MHz cables to protect it from transmitter rf pulses. The ouput of the preamplifier was amplified by an RHG amplifier (LBL 10x1550), then sent to the quadrature phase detector. The reference phase to the quadrature detector could be adjusted to control the output phases of the signal. The phase detected signals from the quadrature phase detector were filtered by the Rockland filters, then recorded by the Nicolet 2090/201 transient recorder and signal averaged on the Nicolet 80 computer. The data were recorded in quadrature.

Both raw data and fourier transformed data were transferred to the VAX.

4.3.3 Generation of logic/data aquisition

A Nicolet-80 computer attached to a modified Nicolet 293 timer running a modified NTCFT verison #1002 program controlled the generation of rf pulses and data aquisition. A Nicolet 2090 with a 201 plug-in first recorded the solid echo or free induction decay, then

transferred the data to the Nic-80 computer. The 2090/201 was needed to record the solid echo because of the Nic-80's limited digitizing rate of 10 μs. NTCFT version #1002 was modified to run with the 2090. An overlay, UD1080 provided by Nicolet, allowed sorting (unshuffling) of overlapping quadrature data as obtained from the 2090. Additional changes to NTCFT are listed in Appendix 2.

10 one-shots were added to the Nicolet 293 timer to give additional flexibility in creating pulse sequences. The connections on the 293 timer patch panel which determined the PENIS and ONP pulse sequences are shown in Appendix 1. The output of the 293 controlled the ^{1}H pulse lengths and phases and the ac relay which controlled the shutter and the flow of N_2 in the PENIS experiment.

In both the PENIS and ONP experiments, the phase of the transmitter pulse was controlled externally. One of the outputs of the 293 went to a pulse sorter which could be programmed to sort up to 16 separate time frames. At the correct time, logic pulses were sent out 4 separate gate lines. In the ONP experiment, these 4 outputs of the sorter went to the 4 pulse generator (LBL 16x608) which contained 4 separate pulse length controls. The 4 outputs of the 4 pulse generator controlled the output phase and length of the transmitter pulse by gating on the appropriate rf phase gate of the quadripolar phase splitter. In th PENIS experiment, the 4 outputs of the pulse sorter went directly to the quadripolar phase splitter.

4.3.4 Lock Channel

The lock channel was designed by Alan Robertson and has been described elsewhere [17]. The magnetic field was locked on the

deuterium signal from an external sample of D_2O.

4.4 Detection and Tune-up

4.4.1 PENIS

^{13}C was detected at 15.1 MHz using the PENIS technique of Pines, et al [3]. The Hartman-Hahn condition was satisfied using the following tune-up procedure. The free induction decays of ^{13}C and ^{1}H in 70% ^{13}C enriched methyl iodide were monitored. The lengths of the 180 degrees ^{1}H and ^{13}C pulses were made equal by adjusting the output power levels of the Bruker amplifier and/or the input to the (LBL 16x970) ^{1}H amplifier. ^{13}C's in adamantane were then cross polarized and the rf levels and contact time adjusted until the maximum signal intensity was detected. In general, the Hartman-Hahn condition was satisfied with a rotating field strength of 48 gauss for ^{13}C and 12 gauss for ^{1}H and a contact time of 5 ms was used.

Ordinarily, for fluorene, 100-200 spectra were signal averaged. The repitition rate was on the order of 1 minute and was limited by the illumination-optical polarization time of the crystal.

4.4.2 ONP

Since the dead time of the receiver system ($\sim$20μs) was greater than T_2, the time constant of the ^{1}H free induction decay in the solid crystal ($\sim$10 μs), protons were detected using the (two-pulse) solid state (dipolar) echo technique, which refocused the spins at a selected time τ after the application of the second pulse [23]. The basic pulse sequence is $90^{0}(\pi/2)$-τ- 90^{0}-τ-[detect]. τ = 20 μs, the dead time of the receiver. A simple description of the echo is given

in Appendix O. Rf transmitter pulse phases were initially checked with an HP vector voltmeter. The 180^{o} pulse length of each phase was determined by monitoring the on-resonance free induction decay of protons in methyl iodide. In general, the 90^{o} pulse time was 2 μs (≈30 gauss protons) with an input of 500 watts. The signal after a 90^{o}-τ-90^{o} sequence (no phase shift) was monitored to check whether the signal intensity was at a minimum. The echo sequence was first used to detect protons in gypsum, $CaSO_4.2H_2O$, as a check of rf phases and pulse lengths.

4.5 Fluorene

4.5.1 Crystal structure

Fluorene crystallizes in the orthorhombic space group D_{2h}^{16} (Pnam), with 4 molecules per unit cell [24]. See fig 4.6. The 4 molecules in a unit cell are pairwise magnetically equivalent, since each member of a pair is related to the other by a screw axis rotation. The long in-plane axis of all 4 molecules is parallel to the c axis of the crystal. The molecule posseses a mirror plane of symmetry which is parallel to the ab crystal plane. The planes of the molecules are inclined ±34.5 degrees from the crystal b axis.

4.5.2. Crystal growth

Synthesized fluorene was generously donated by Herbert Zimmerman. Acridine was zone refined by Sydney Wolfe. Fluorene crystals doped with 1000 ppm acridine were grown from the melt by Sydney Wolfe using the Bridgman technique [25].

Commercial fluorene, even after repeated zone refining, contained anthracene and benz-f-indane and was unsuitable for ONP experiments [1,26]. Although optically generated ^1H signals could be produced and detected, the time constant for the optical polarization was exceedingly long (>>5 minutes). The ONP signals measured during the first 1-2 minutes of illumination time were two orders of magnitude lower in intensity than the signals detected from pure synthesized fluorene.

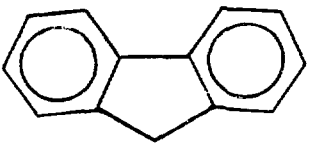

fluorene

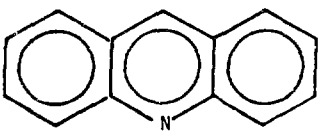

acridine

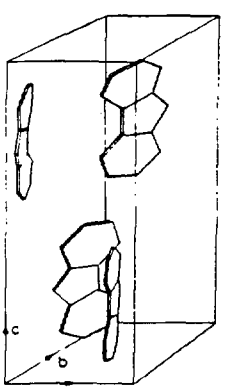

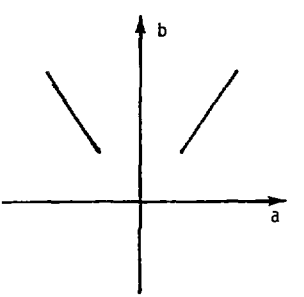

Figure 4.6 Top: molecular structure fluorene and acridine. Bottom,left: crystal structure. Bottom, right: schematic representation 2 magnetically inequivalent molecules in ab crystal plane.

5. DATA ANALYSIS

5.1 Background

The magnetic shielding Hamiltonian of a nuclear spin S in an external magnetic field Ho is

$$H_S = \gamma Ho \cdot \sigma \cdot S \qquad 5.01$$

where σ is the second rank chemical shielding tensor representing the interaction of the nuclear spin with the surrounding electrons. In a single crystal the resonance frequency of the spin S is a function of the orientation of the external magnetic field with respect to the crystal. Since the eigenstates of the full Hamiltonian are S parallel Ho and S anti-parallel to Ho, the NMR experiment determines only certain elements of σ.

Let the laboratory frame be defined by the coordinate axes 1,2,3. Ho is in the 2-3 plane, parallel to the 3 axis. See figure 5.1. Let the chemical shift tensor in this laboratory frame, σ_{lab}, be represented by the symmetric matrix

$$\begin{bmatrix} \sigma_{11} & \sigma_{12} & \sigma_{13} \\ \sigma_{21} & \sigma_{22} & \sigma_{23} \\ \sigma_{31} & \sigma_{32} & \sigma_{33} \end{bmatrix} \qquad 5.02$$

Let $R_{xtl \rightarrow lab}$ be the rotation matrix which transforms the chemical shielding tensor in the crystal frame, σ_{xtl} to the laboratory 1,2,3 frame, i.e.

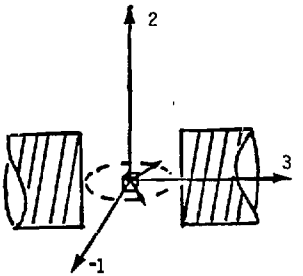

laboratory frame

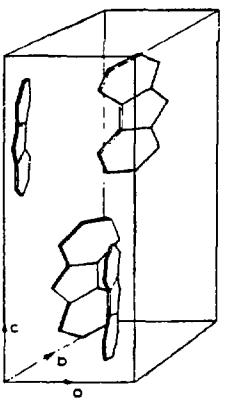

crystal frame

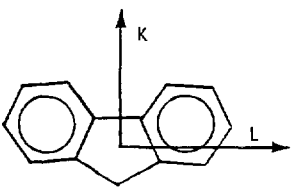

molecular frame

Figure 5.1 Orientation of various coordinate systems as used in data analysis.

$$\sigma_{lab} = R_{xtl \rightarrow lab} \cdot \sigma_{xtl} \cdot R^{-1}_{xtl \rightarrow lab} \qquad 5.03$$

Expressed in terms of the standard Euler angles α, β and ψ, a rotation matrix R is given by,

$$R = \begin{bmatrix} \cos\alpha\cos\beta\cos\psi - \sin\alpha\sin\psi & \sin\alpha\cos\beta\cos\psi + \cos\alpha\sin\psi & -\sin\beta\cos\psi \\ -\cos\alpha\cos\beta\sin\psi - \sin\alpha\cos\psi & -\sin\alpha\cos\beta\sin\psi + \cos\alpha\cos\psi & \sin\beta\sin\psi \\ \cos\alpha\sin\beta & \sin\alpha\sin\beta & \cos\beta \end{bmatrix}$$

where α is a rotation about the original z axis, β is about the new y axis, and ψ is about the final z axis.

The crystal is mounted in a particular orientation and rotated about the laboratory 2 axis. The component of σ_{lab} which is parallel to the magnetic field Ho, σ_1, is measured as a function of rotation angle u, i.e., since Ho // 3,

$$\sigma_1 = n \cdot R_2 \cdot \sigma_{lab} \cdot R^{-1}{}_2 \cdot n^T \qquad 5.05(a)$$

where σ_{lab} is the symmetric matrix given above and

$$n = (0,0,1)$$

$$R_2 = \begin{bmatrix} \cos(u) & 0 & -\sin(u) \\ 0 & 1 & 0 \\ \sin(u) & 0 & \cos(u) \end{bmatrix}$$

Therefore,

$$\sigma_{lab} = A + B\cos(2u) + C\sin(2u) \qquad 5.05(b)$$

where

$$A = {}^1/_2 \, (\sigma_{11} + \sigma_{33})$$

$$B = {}^{1}/_{2}\,(\sigma_{33} - \sigma_{11})$$

$$C = \sigma_{13} \qquad (\sigma_{ij}=\sigma_{ji})$$

A curve, called a rotation plot, is fitted to equation 5.05 to determine the coefficients A, B and C, and hence the elements $\sigma_{11}, \sigma_{33}, \sigma_{13}$ of σ_{lab}. σ_{xtl} at this point is underdetermined.

The crystal is remounted and again rotated about the laboratory 2 axis. Let $R'_{xtl\rightarrow lab}$ be the (second) rotation matrix which transforms σ_{xtl} to the laboratory frame, i.e.

$$\sigma'_{lab} = R'_{xtl\rightarrow lab} \cdot \sigma_{xtl} \cdot R'^{-1}_{xtl\rightarrow lab} \qquad 5.06$$

The chemical shift as a function of rotation angle u is again measured.

The coefficients from the rotation plots from the j crystal mountings (orientations) can be written as,

$$\begin{aligned} A(n) &= {}^{1}/_{2} \Sigma_{kl}\, \sigma_{kl}[R(n)_{1k}R(n)_{11} + R(n)_{2k}R(n)_{21}] \\ B(n) &= {}^{1}/_{2} \Sigma_{kl}\, \sigma_{kl}[R(n)_{1k}R(n)_{11} - R(n)_{2k}R(n)_{21}] \\ C(n) &= {}^{1}/_{2} \Sigma_{kl}\, \sigma_{kl}[R(n)_{1k}R(n)_{21} + R(n)_{2k}R(n)_{11}] \\ n&=1,j \end{aligned} \qquad 5.07$$

where the $R(n)_{ij}$s are the elements of the nth rotation matrix R which transforms σ_{xtl} to the laboratory frame (i.e., elements of $R_{xtl\rightarrow lab}$ and $R'_{xtl\rightarrow lab}$) and the σ_{kl}s are the elements of σ_{xtl}, σ in the crystal frame.

The chemical shift measurements are repeated, and correspondingly, the coefficients of the rotation plots determined, until all elements of σ_{xtl} are determined. The tensor is then

diagonalized to yield the values of the principal elements and the orientation of the principal axes. Figure 5.1 depicts the various coordinate systems used in this text.

5.2 Analysis

The data were analyzed by methods outlined by Mehring [27]. The data analysis fell into three parts:

i) the orientations of the crystal a,b,c axes with respect to the laboratory coordinate system were determined with the crystal mounted in two separate orientations. (The laboratory frame was as described above: Ho was parallel to the 3 axis; the crystal was rotated about the axis perpendicular to Ho, the 2 axis; the 1 axis was perpendicular to axes 2 and 3.) The orientations of the molecules in the unit cell were known from x-ray diffraction.

ii) for each orientation of the crystal, the observed chemical shift σ_1 as a function of rotation angle, u, was fitted to equation 5.05 by least squares analysis to determined the coefficients A,B,C;

iii) by least squares analysis, the two sets of coefficients (A(1),B(1),C(1) from orientation 1 and A(2),B(2),C(2) from orientation 2) obtained from (ii) were fitted to equation 5.07 using orientation information from (i). Tensors were determined in the molecular coordinate system, defined by the axes k,l,m. (See figure 5.1). In this case, the R_{ij}s are elements of the rotation matrices which make the laboratory coordinate system and the molecular coordinate system coincident for the two different orientations of the crystal; σ_{ij}s are the elements of σ in the molecular frame.

5.2.1 Determination of crystal orientation

The orientation of the crystal axes with respect to the laboratory axes for the two different mountings of the crystal was determined differently.

In orientation 1, the crystal ab plane was chosen to be perpendicular to the rotation axis. This was called the ab plane orientation. Since the ab plane is the cleavage plane of the crystal, to reach this orientation, the crystal was first mounted with the cleavage plane approximately perpendicular to the rotation axis. The maximum ONP is observed when the magnetic field is oriented 10^{o} away from the a axis in the ab plane. To reach the ab plane orientation, the proton ONP was measured and the crystal orientation was adjusted until the ONP signal was maximized and the intensity of the signals 180^{o} apart was approximately equal.

In orientation 2, the crystal ac plane was chosen to be roughly perpendicular to the rotation axis. The crystal was mounted in the NMR tube with the cleavage plane approximately parallel to the rotation axis. X-ray diffraction was then used to determine the orientation of the crystal axes with respect to the tube axis. The ac plane was found to be tilted approximately 16^{o} with respect to the plane normal to the rotation axis.

5.2.2 Rotation plots

For each of the two approximately orthogonal crystal orientations described above, rotation plots of the chemical shift σ_1 as a function of rotation angle u were made. To make the rotation plots, ^{13}C spectra were taken and the positions of peaks recorded at

approximately 10^{0} intervals over a 180^{0} range. Typical spectra from orientations 1 and 2 are shown in figure 5.2.

The major difficulty of the analysis was untangling the various peaks and determining which peaks belonged to which chemical shift tensor.

The maximum number of lines (peaks) in a typical fluorene carbon spectrum can be calculated from the crystal structure of fluorene. One line results from each carbon atom tensor on each of the two molecules, giving a total of 26 lines.

The ab plane is parallel to the the molecular mirror plane. Therefore, in the ab plane orientation, the two halves of the molecule are magnetically equivalent. This reduces the number of possible lines, and the corresponding number of incongruent chemical shift tensors to 14: 1 methylene bridge carbon tensor and 6 aromatic carbon tensors from each of the two molecules.

In orientation 2, all 26 lines were possible, but due to the heavy overlap of peaks not all 26 separate lines were observed.

For both orientations, least squares fits were done to extract the coefficients A,B,C from the rotation plots using IMSLS subroutine ZXSSQ [28]. Coefficients from a fit were considered acceptable if the fit had a reduced chi-squared of less than 2, i.e., $\chi_r < 2$. In orientation 1, 14 acceptable curves were found; in orientation 2 > 26 acceptable curves were found. All curves were kept at this stage of the analysis.

5.2.3 Full tensor fit

Since data were taken for only two orientations of the crystal,

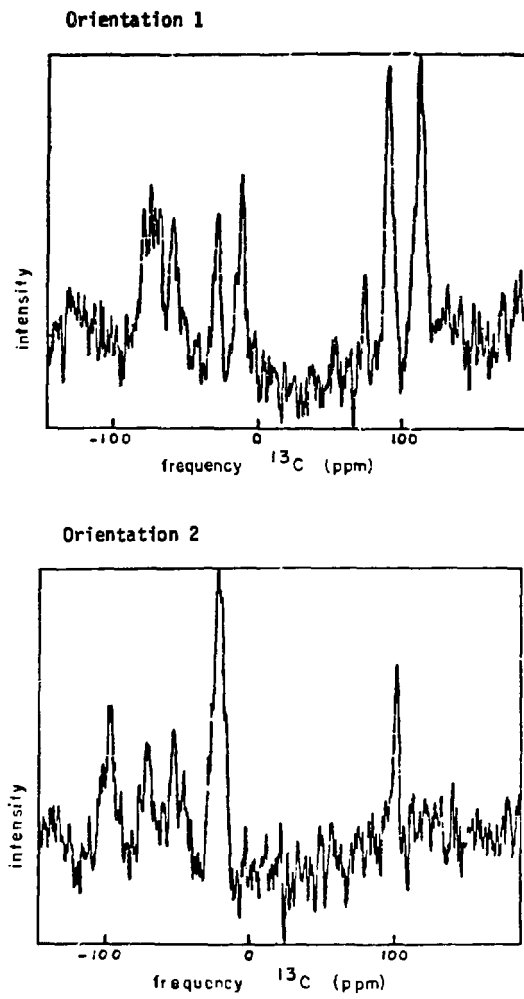

Figure 5.2 Typical spectra ^{13}C. Top: ab plane orientation
Bottom: "~ac" plane orientation.

the chemical shielding tensors in the crystal frame were underdetermined. The tensors of the carbons of the two molecules were assummed to be identical. Rotation plots from these carbon tensors were combined for the least squares fit of equation 5.07. In addition, for the aromatic carbon tensors, the orientation of one of the principal axes was assumed to be perpendicular to the plane of the molecule. The methylene carbon tensor was also calculated with the orientation of one principal axis pre-determined.

For each of the 6 incongruent aromatic tensors, 2^3=8 rotation curves were possible: 2 orientaions x 2 inequivalent molecules per orientation x 2 equivalent tensors per molecule (due to the mirror symmetry plane). However, in orientation 1, the ab plane orientation, the rotation plots of the two equivalent tensors on each molecule were coincident. A total of 6 rotation curves for each of the 6 incongruent aromatic tensors was therefore possible. For the methylene carbon, a total of 2^2=4 rotation curves was possible: 2 orientations x 2 inequivalent molecules per orientation.

Rotation curves produced by the same tensor in different orientations were determined in the following way. The line of intersection of the two orientation planes was determined. The spectrum taken here must be identical in both orientations. Those rotation curves from the two different orientations which go through the same peak at this line of intersection belong to the same tensor.

Rotation curves of identical tensors on different molecules were determined in the following way. Since the ab plane contains the molecular symmetry plane, the two halves of the molecule are magnetically equivalent when the magnetic field lies in this plane.

Moreover, in this orientation, the two inequivalent molecules are related by a rotation about the c axis by 69^{o}. The rotation curves of the ab plane orientation reflected this crystal symmetry, i.e., there were two sets of rotation curves, one phase shifted from the other by 69^{o}. This can be easily seen in figure 5.3. Curves with the same maximum chemical shift belong to identical tensors on different molecules.

The orientation Rijs were known from (i) and the rotation plot coefficients from (ii). IMSLS routine ZXSSQ was used to fit the sets of coefficients from orientations 1 and 2 to equation 5.07.

Many of the rotation curves whose coefficients were used to calculate a tensor resulted in fits with $\chi_r > 5$ and were discarded. Only fits with $\chi_r < 2$ were kept. All the rotation curves which were kept are shown in figures 5.3 and 5.4. The rotation curves which were used to fit each of the 7 incongruent tensors are shown in figures 5.5 through 5.12 along with the associated carbon. Note that the number of rotation plots used for the full tensor fit was less than the number of possible rotation plots. Due to the larger statistical error in orientation 2, (see section 6.2.2.1) the number of rotation plots used here for each tensor fit was less than the total possible rotation plots. In the ac plane orientation either i) two rotation plots from one molecule or ii) two rotation plots from molecule 1 and one rotation plot from the molecule 2 were used. This minimized χ_r.

Aromatic tensor components were calculated with respect to the molecular coordinate system, defined by axes k,l,m. See figure 5.1. One principal axis was assumed to be perpendicular to the plane of the

molecule (σ_{mm}). For case (i), 4 sets of coefficients (i.e. 12 equations) and for case (ii), 5 sets of coefficients (i.e.15 equations) were used to fit 4 unknowns, the elements σ_{kk}, σ_{kl}, σ_{ll}, and σ_{mm} (the perpendicular to the molecular plane) of the chemical shift tensor in the molecular coordinate system. σ_{kk}, σ_{kl} and σ_{ll} were then used to determine the values of the other principal elements and their orientations. The results of both fits (either case i or ii) were identical.

The methylene tensor was also calculated with respect to the molecular coordinate system. The calculations were done assuming either:

i) one of the principal axes was oriented in the C-C-C bond plane, bisecting both the C-C-C bond the the CH_2 bond (along molecular axis k); or

ii) one of the principal axes was oriented perpendicular to the plane of the molecule (along axis m); or

iii) one of the principal axes was oriented perpendicular to the CH_2 plane.

The results were as follows:

The values of the principal elements did not change with each assumption.

With assumption (i), the other principal axes were rotated an angle of $5^{o} \pm 12^{o}$ away from the moleclar l and m axes (rotation about the molecular about the molecular k axis).

With assumption (ii), the direction of the other principal axes were rotated $9^{o} \pm 21^{o}$ away from the molecular k and l axes (about the molecular m axis).

With assumption (iii), the other principal axes were rotated $11^{0} \pm 26^{0}$ about the molecular 1 axis.

X-ray diffraction studies have shown that the fluorene molecule is planar and posseses C_2 symmetry [24]. In addition, the proton-proton vector of the methylene carbon has been shown to be perpendicular to the molecular plane [2]. Therefore, considering the symmetry of the molecule, the orientation of the methylene carbon bonds and the results of the above calculations, the orientation of the principal axes was taken to be, to first order, roughly coincident with the molecular coordinate system.

As a check of the full tensor calculations, the rotation plots from the ab plane (orientation 1) were studied. The largest (positive) values for each of the aromatic tensor rotation curves were found to be equal, within experimental error, to the calculated values of σ_{33}. Moreover, the maximum aromatic chemical shift should be measured when the magnetic field is perpendicular to the fluorene molecular plane. From x-ray diffraction, the vector normal to the fluorene molecular plane is in the ab plane, rotated 69^{0} away from the b axis. The largest (positive) values for the rotation curves produced by the aromatic carbon tensors were found to be at the angle $\arctan(C/B) = 68^{0} \pm 3^{0}$, in agreement with the expected value. $\pm 3^{0}$ represents the error in orienting the crystal in the ab plane.

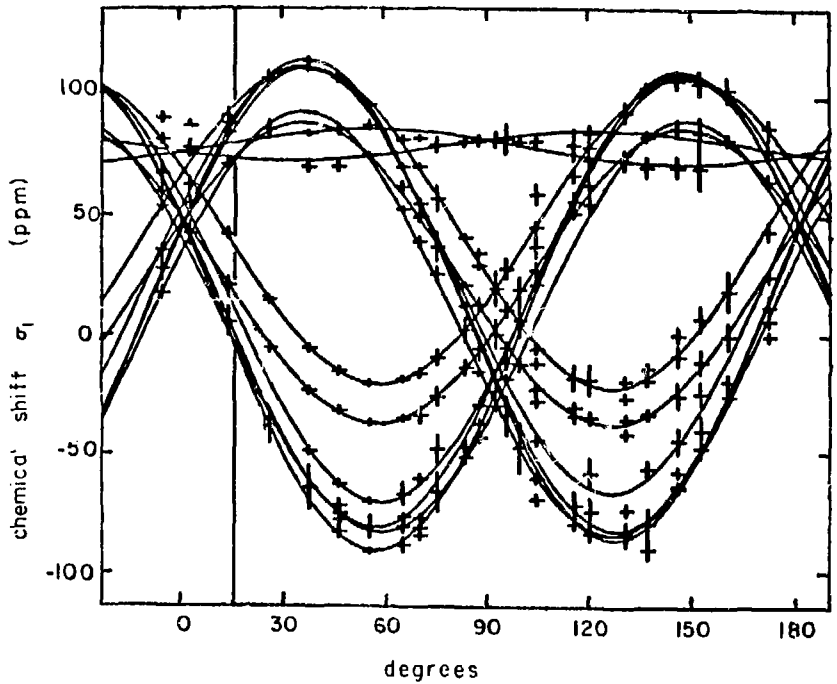

Figure 5.3 ab plane rotation curves. Vertical line denotes line of intersection with " ac" plane.

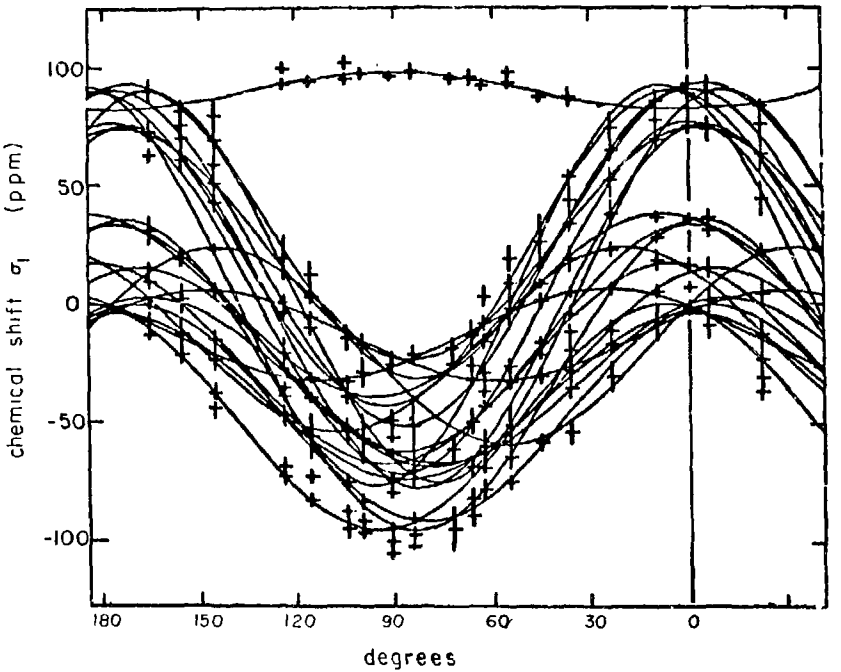

Figure 5.4 "ac" plane rotation curves. Vertical line denotes line of intersection with ab plane.

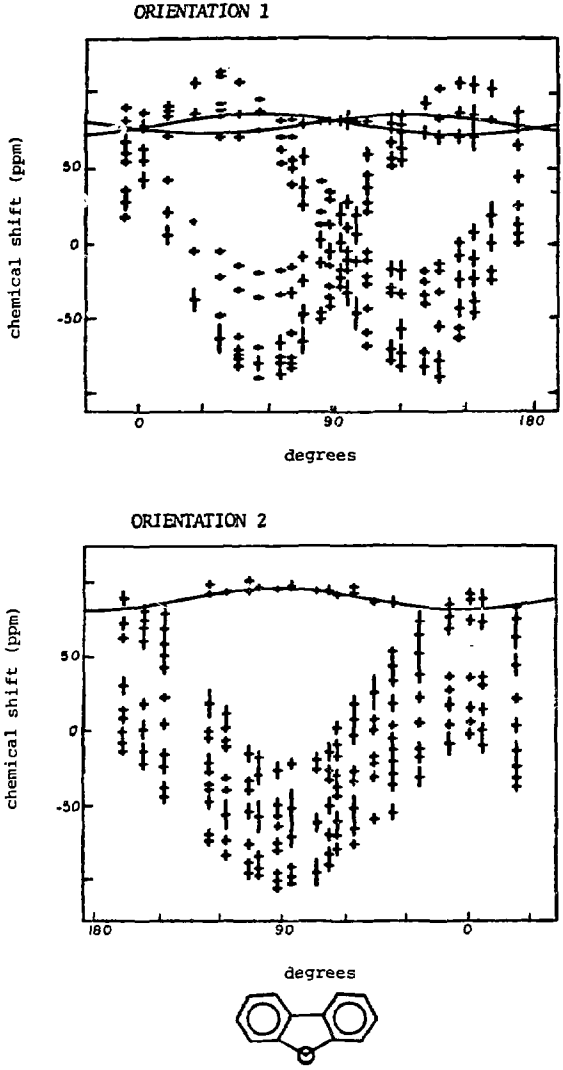

Figure 5.5 Rotation curves, Cl

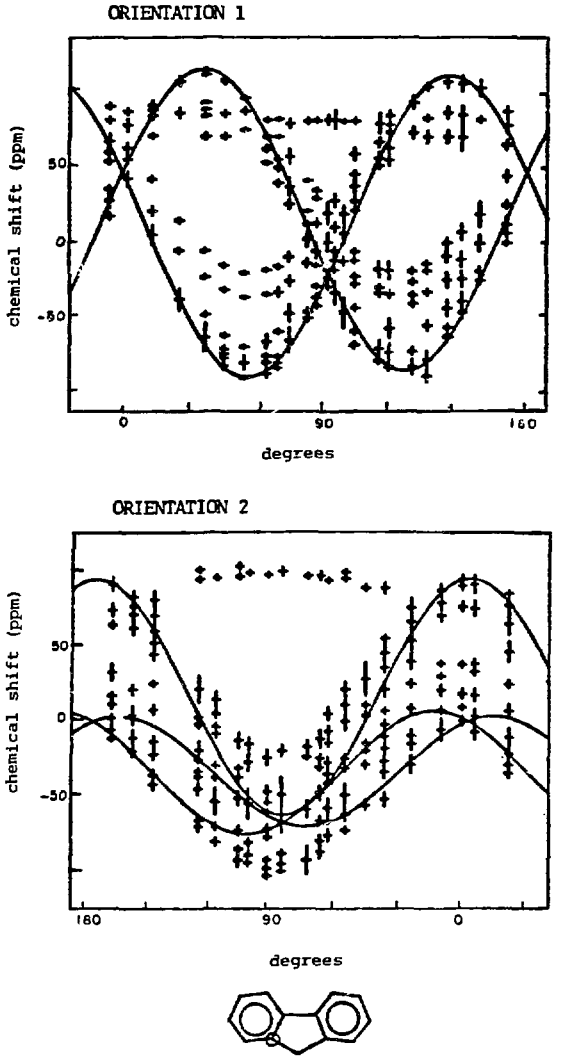

Figure 5.6 Rotation curves, C2

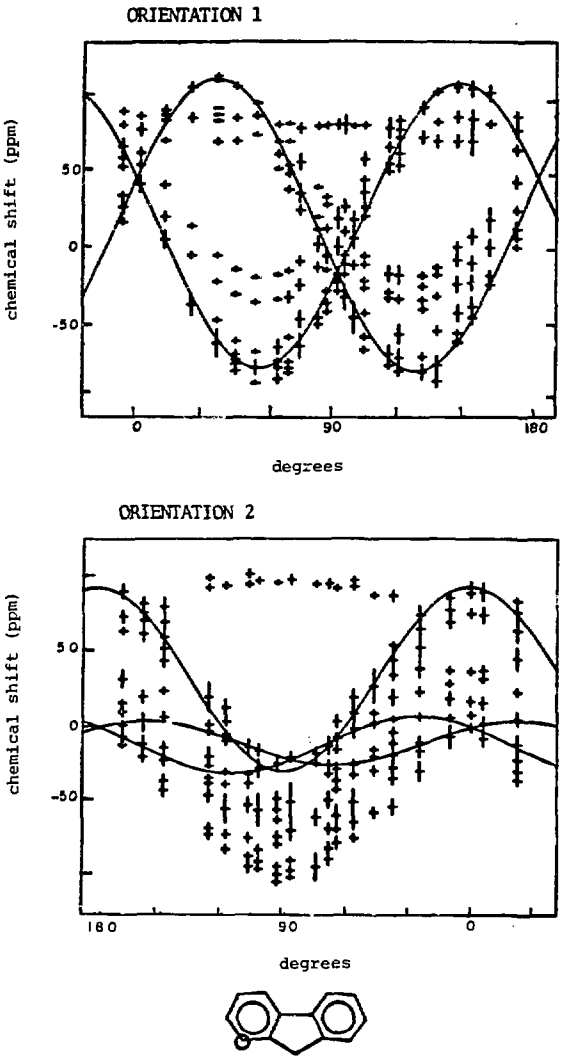

Figure 5.7 Rotation curves, C3

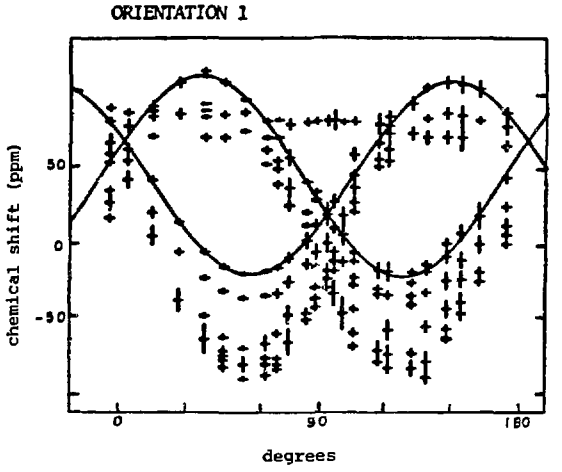

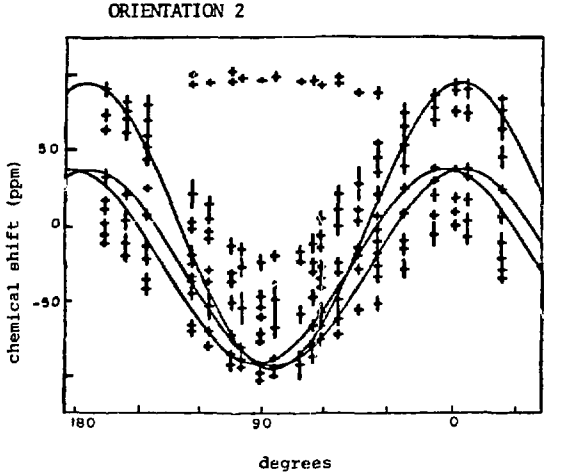

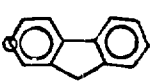

Figure 5.8 Rotation curves C4

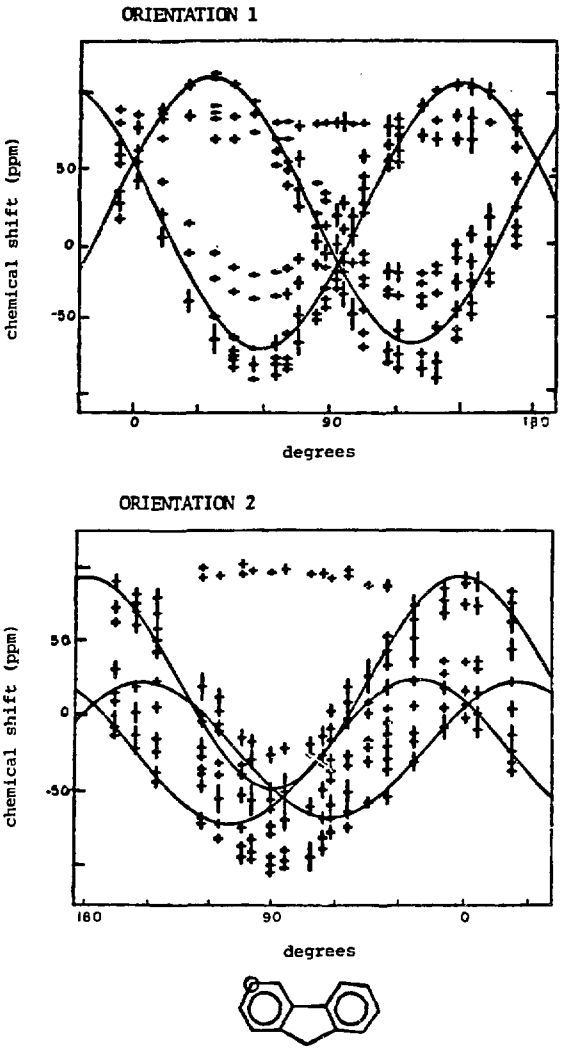

Figure 5.9 Rotation curves, C5

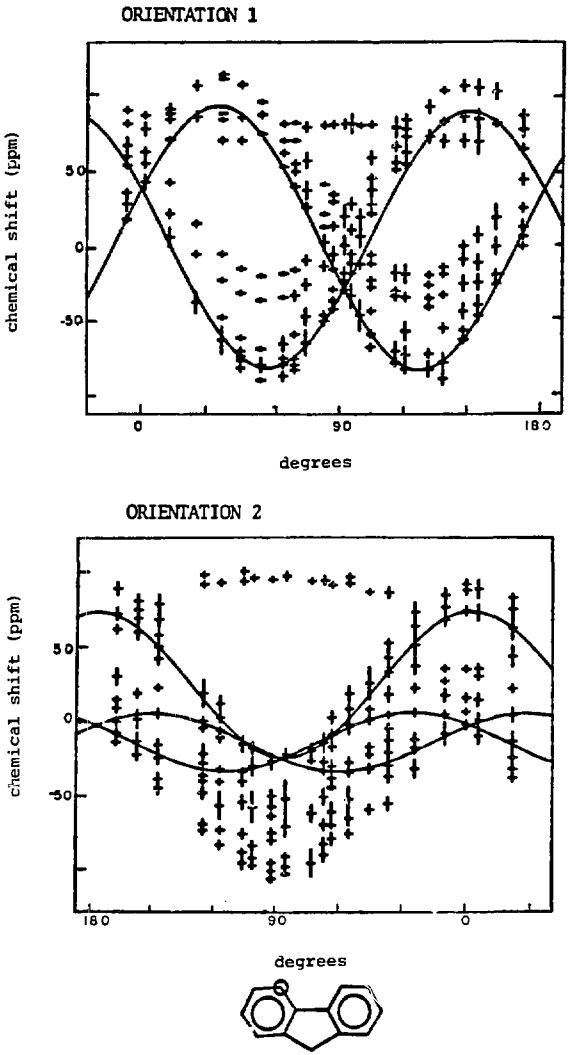

Figure 5.10 Rotation curves, C6

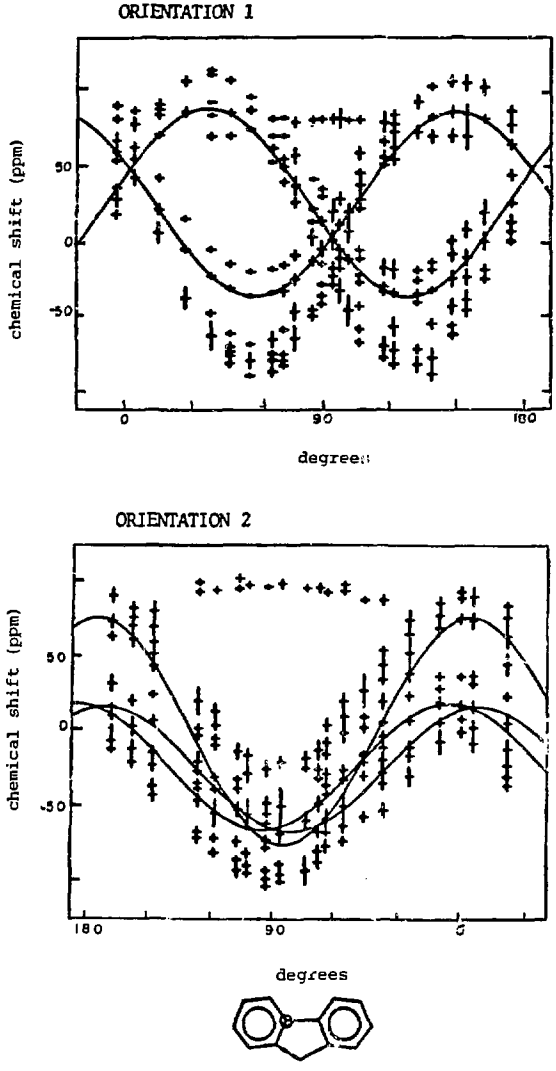

Figure 5.11 Rotation curves, C7

6. RESULTS

6.1 ONP

6.1.1. Single crystal

For selected orientations of the acridine-doped fluorene single crystal, the optically generated proton polarization is approximately 100 times greater than the Boltzmann polarization generated at room temperature in a 14.1 kGauss magnetic field.

Figure 6.1 plots the growth of proton polarization of the fluorene single crystal as a function of illumination time for a particular light intensity and orientation. The growth is exponential.

Figure 6.2 shows a typical proton NMR spectrum of the fluorene single crystal. The crytal is oriented with respect to the magnetic field to yield the maximum ONP signal. The illumination time here is approximately one minute. The line width is 35 khz, 9 gauss.

Figure 6.3 shows the intensity of the optically generated signal over a restricted angular range where the ONP signal is maximal.

The optically generated polarization is of comparable magnitude to the polarizations reported by Stehlik, et al [9], using a 1600 watt Xe lamp. The magnitude of the signal depends critically upon the light intensity; dp/dt depends linearly upon the light intensity. The 1000 watt Xe-Hg bulb has an intrinsically higher luminosity at uv wavelengths than the 1600 Xe or the 100 watt Hg lamps used by Stehlik, et al [29] and one might expect that larger polarizations would be generated. However, the condensing system used

here is smaller than that used by Stehlik, et al [11,30] and therefore less light is collected. The 1000 watt Xe-Hg lamp has a much larger arc than the 100 watt Hg lamp and cannot be focused down to as small an image size. In addition, the crystal may not have been optimally oriented to produce the maximum ONP signals; it may have been mis-oriented by $\pm\sim 3^{o}$ (see section 5.2.3). (Care was taken to orient the crystal in the ab plane.) More care could be taken to maximize the light intensity illuminating the crystal--larger diameter collecting,focusing lens, shorter light pipe, etc.

Note that the magnitude of the polarization reported here is for the fully protonated fluorene/acridine system. The polarizations are approximately an order of magnitude smaller than for the fluorene,d_8h_2-acridine,h_9 cystals reported by Stehlik, et al [1,2].

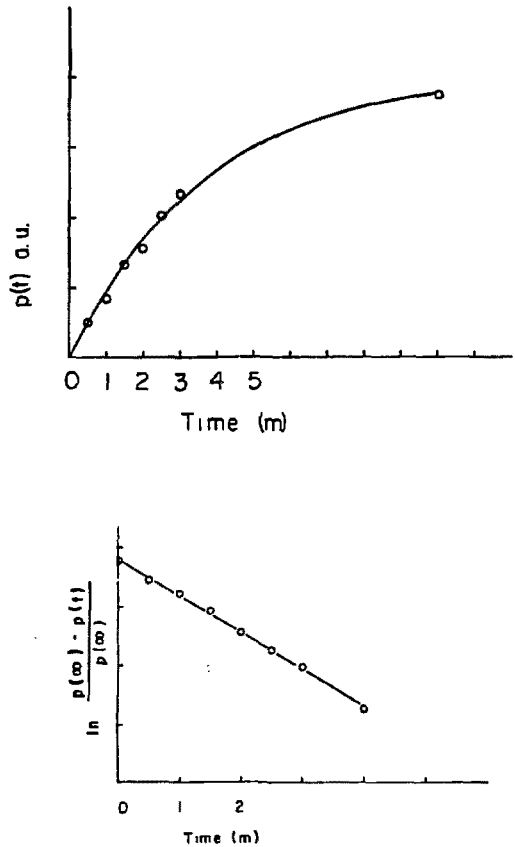

Figure 6.1 dp/dt. Proton polarization growth as a function of time.

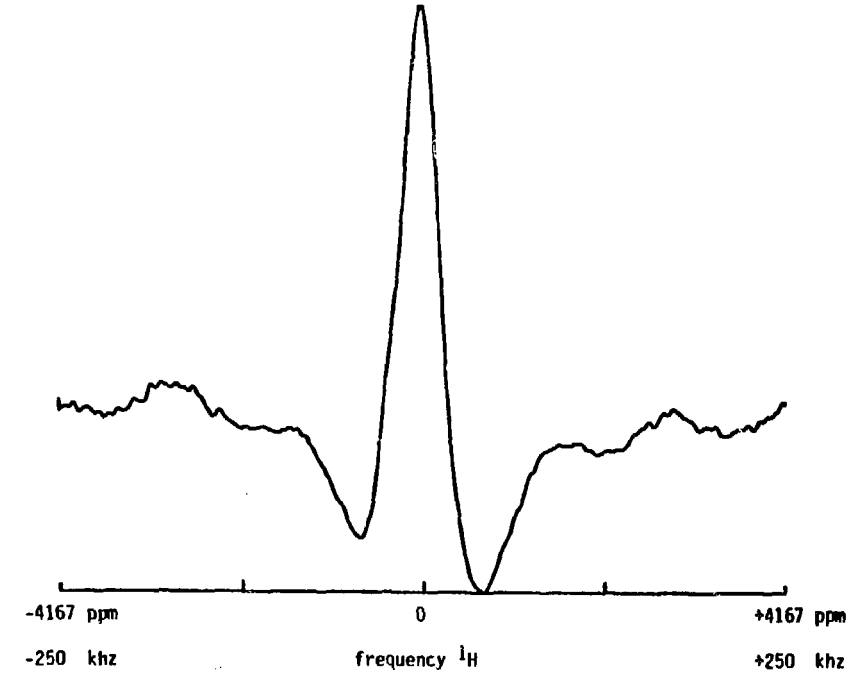

Figure 6.2 Typical spectrum proton ONP: single crystal, acridine-doped fluorene.

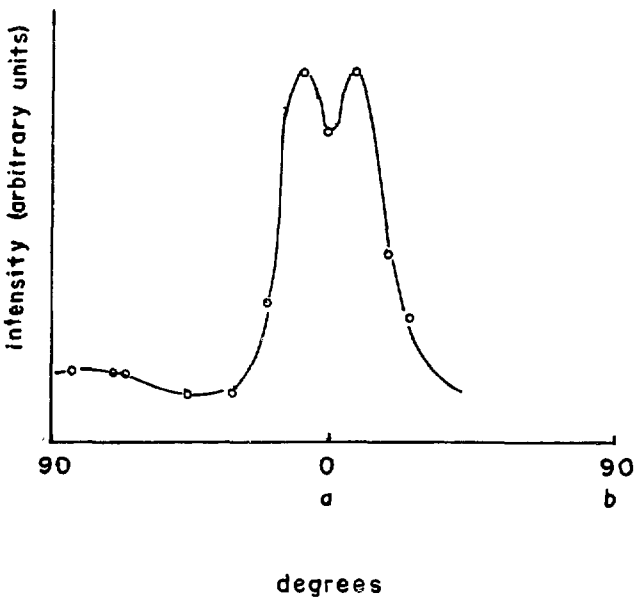

Figure 6.3 Proton ONP as a function of field orientation in ab plane, near maximum ONP signal. Hp = 80 gauss.

6.1.2. Powder samples

In general, many compounds do not crystallize easily or do not form large crystals suitable for NMR experiments. Powdered and randomly dispersed samples are generally far more readily avaliable than single crystals. Studies of powdered samples of acridine-doped fluorene appeared to be the next step in the attempt to create large ^{1}H polarizations, and hence, ^{13}C polarizations, in a typical NMR system.

Optically generated proton signals in powdered samples of acridine-doped fluorene have been detected. Figure 6.4 shows a typical optically generated proton NMR powder spectrum. The intensity of the signal as a function of field strength over a restricted field strength region where the ONP is maximal is shown in figure 6.5 The powder ONP signals are approximately of the same amplitude as the 14 kGauss Boltzmann generated signals. This measured intensity is approximately 10 times smaller than what is expected.

In a field of 80 gauss, the proton ONP of a single crystal can be measured as a function of orientation of the crystal axes with respect to the magnetic field (for example, see figure 6.3). The single crystal ONP is maximal when the magnetic field is oriented in the ab plane, 10^{o} away from the a axis. The measured ONP about this restricted angle is far greater than at any other orientation of the crystal.

To first order, the ONP of the powdered sample is determined by that fraction of sample with the a axis oriented within approximately 20^{o} of the magnetic field direction. Furthermore, assuming a uniform ONP of 100 x Boltzmann for the crystallites in such an orientation,

the ONP of the powdered sample should be approximately fraction (1/10) x polarization (100 x Boltzmann) = 10 x Boltzmann.

The measured intensity is lower than that predicted probably because of the large amount of light scattering produced by the tiny crystallites, reducing the effective illumination of the sample. A powdered sample cannot be illuminated as well as a cleaved single crystal. Since the polarization is dependent upon the light intensity, the powdered sample, with its reduced illumination, would not have as large a polarization.

Attempts to reduce the light scattering were unsuccessful. Attempts to fuse the powder into a clear wafer proved unsuccessful. Also, the solid material could not be refractive index-matched: it dissolves quite well in various oils and solvents.

Although the optically generated signals of the powdered samples are not large, they can be generated and measured in a time less than than T_1, the proton spin lattice relaxation time in the dark. T_1 of the fluorene protons in the dark is >30 minutes @ 14 kGauss [31]. The equilibrium Boltzmann magnetization @ 14 kGauss is generated is a time 3-5 x T_1, on the order of an hour. Optically generated magnetization can be measured in 10's of minutes, the time determined by the illumination time of the sample.

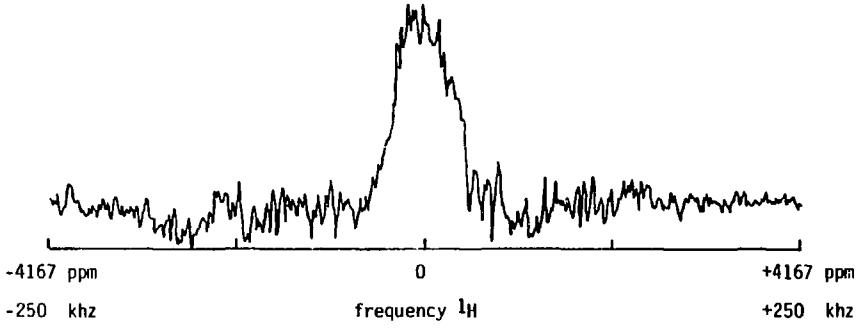

Figure 6.4 Optically polarized ^1H: powder, acridine-doped fluorene

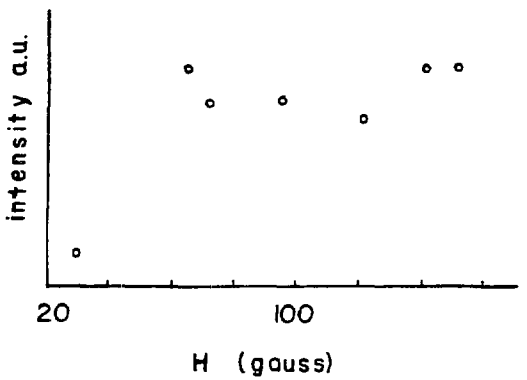

Figure 6.5 Proton ONP as a function of polarization field: powder, acridine-doped fluorene

6.2 PENIS

ONP of protons in combination with the PENIS double resonance experiment produces large ^{13}C signals in fluorene single crystals. The ^{13}C signal is estimated to be 400 times larger than the normal Boltzmann ^{13}C signal generated at room temperature in a 14.1 kGauss magnetic field.

Figure 6.6 shows a ^{13}C 1-contact PENIS spectrum of the fluorene single crystal, obtained by first optically polarizing the protons. Since attempts to measure the normal Boltzmann ^{13}C signals directly and attempts to cross polarize the ^{13}C using the normal Boltzmann proton reservoir were both unsuccessful, the estimate of the gain in ^{13}C polarization is determined in the following way. First, the ^{13}C signal is observed to be roughly directly proportional to the proton ^{1}H signal. This linear dependence can be observed by varying the intensity of the light illuminating the sample, hence, varying the proton polarization, and measuring the cross polarized ^{13}C signal. Second, cross polarized ^{13}C signals in adamantane are observed to be 4 times larger than their Boltzmann polarization when in contact with their normal Boltzmann proton reservoir. Since the optically generated proton signal is approximately 100 times greater than the normal Boltzmann polarization, the resultant gain is approximately 4 x 100. This gain is roughly in accordance with expectations.

Although the proton polarization is large and is not depleted after one contact with ^{13}C, multiple contacts under matched Hartman-Hahn conditions and one-shot PENIS experiments under unmatched Hartman-Hahn conditions were not generally done because the high rf power levels and long contact and data acquisition times could fry the

probe components.

Attempts to cross polarize the carbons using simply the proton Boltzmann population proved unsuccessful for two reasons:

i)the proton Boltzmann spin temperature is 100 times smaller than the optically polarized spin temperature;

ii)the spin lattice relaxation time, T_1, of the fluorene protons in the dark is > 30 minutes @ 14 kGauss [31].

Optical polarization of the protons is necessary to short circuit the long T_1 and to build up the proton reservoir. More important, maximum proton polarization is needed to produce a measurable carbon signal. As can be seen in figure 6.3, rotating the crystal approximately 20 degrees away from one of the maximum ONP positions decreases the proton signal-- and in effect, the proton reservoir--by a factor of three. It would take an order of magnitude longer to accumulate the same spectrum without the maximum optical proton polarization. Since an average spectrum taken under optimum conditions requires 2-3 hours to accumulate, any dimunition of a proton polarization would make the experiment extremely difficult.

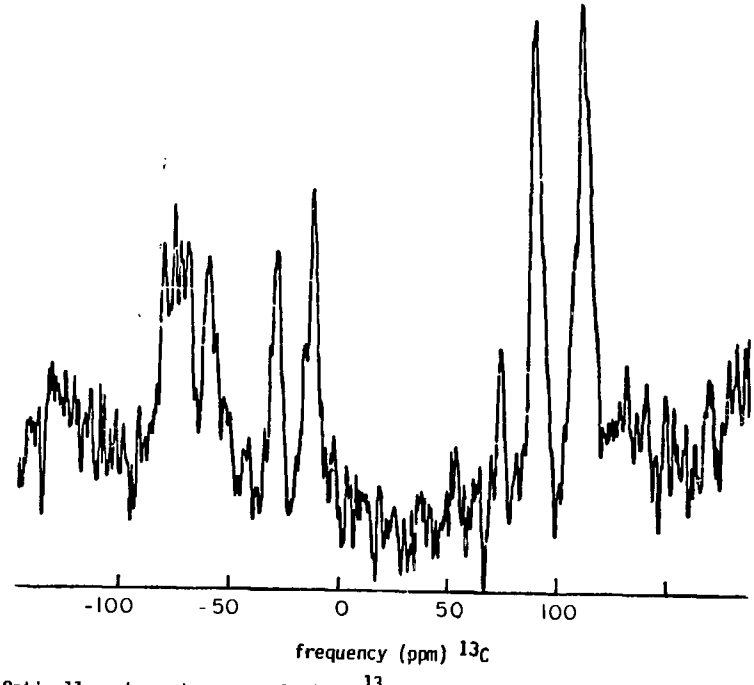

Figure 6.6 Optically enhanced cross polarized ^{13}C spectrum: single crystal, acridine-doped fluorene

6.3. Chemical shift tensors

6.3.1 Tensors

A schematic representation of the seven incongruent ^{13}C shift tensors is shown in figure 6.7. Table 6.1 lists the actual values of the principal elements and their orientation in the molecular plane. Table 6.2 lists the directions cosines of the principal axes with respect to to crystal axes.

There are three different types of carbons, each with characteristically different tensors:

i) aromatic carbons bonded to hydrogen

ii) fused aromatic carbons, i.e. aromatic carbons bonded to another carbon rather than hydrogen

iii) methylene carbon.

All elements of all of the tensors were calculated using the methods outlined in the data analysis section. Values for the principal elements of the tensors could not be obtained from the powder spectra since attempts to cross polarize powder samples were unsuccessful.

Tensor assignments were made following "common sense" arguments: the orientation of the tensors would be generally consistent with those determined by others; for each tensor, $\bar{\sigma}$ would be, within experimental error, equal to σ_i.

6.3.1.1 H-bonded aromatic carbon (C3,C4,C5,C6)

For all of the H-bonded aromatic carbon tensors, the mean value of the principal elements, $\bar{\sigma}=1/3(\sigma_{11}+\sigma_{22}+\sigma_{33})$, agrees within experimental error with the measured isotropic chemical shift σ_i

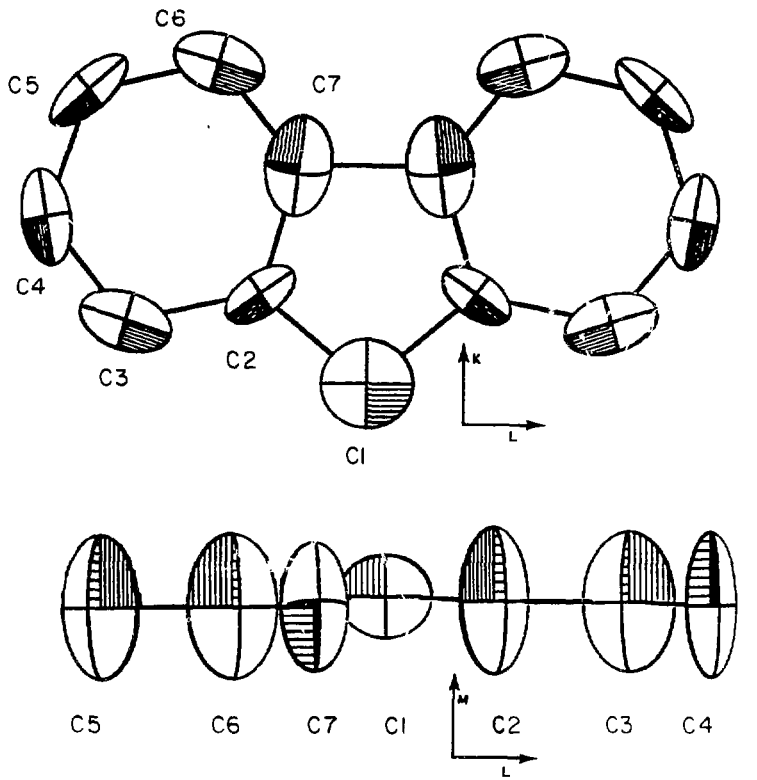

Figure 6.7 Schematic representation of the incongruent carbon shielding tensors of fluorene. The reference 0 for the aromatic tensors is taken to be 120 ppm downfield from the resonance of neat liquid benzene; reference 0 for the methylene carbon is taken to be the resonance of neat liquid benzene. Tensors are represented by ellipsoids, with the shortest axis being the most downfield compenent of the tensor. Labels are as used in text.
Top: orientation of tensors in molecular plane
Bottom: orientation of tensors in plane perpendicular to molecular plane. Molecule rotated 90^0 from top diagram.

Table 6.1

carbon	σ_{11}	σ_{22}	σ_{33}	$\bar{\sigma}$	σ_i*	θ+
C1	76 (3)	90 (3)	102 (4)	89 (2)	91	**
C2	-99 (9)	-47 (9)	119 (5)	-9 (5)	-14	-35^0 (5)
C3	-84 (8)	-12 (5)	97 (3)	1 (3)	4	17^0 (6)
C4	-92 (5)	-14 (6)	114 (4)	3 (3)	2	80^0 6)
C5	-102 (10)	-10 (9)	115 (5)	1 (5)	2	-41^0 (3)
C6	-83 (7)	-17 (7)	116 (5)	5 (4)	9	16^0 (6)
C7	-71 (6)	-27 (8)	93 (2)	-2 (3)	-12	-70^0 (9)

All shifts relative to neat liquid benzene. Errors given in parenthesis.

*ref 48 solvent is either $CDCl_3$ or DMSO-d_6

+rotation angle about molecular M axis to make molecular axis coordinate system and principal axis system coincident (see figures 5.1, 6.7)

** σ_{11} coincident with molecular M axis; σ_{22} with K axis; σ_{33} with L axis (see figures 5.1, 6.7)

Table 6.2

carbon	direction cosines (relative to crystal axes)			principal value (ppm)
c1	-0.566	0.0	-0.824	75
	0.824	0.0	-0.566	89
	0.0	-1.0	0.0	103
c2	-0.464	0.324	-0.824	- 99
	0.675	-0.472	-0.566	- 47
	-0.574	-0.819	0.0	119
c3	-0.542	-0.166	-0.824	- 84
	0.788	0.241	-0.566	- 12
	0.292	-0.956	0.0	97
c4	-0.010	-0.558	-0.824	- 92
	0.143	0.812	-0.566	- 14
	0.984	-0.174	0.0	114
c5	-0.427	0.372	-0.824	-100
	0.622	-0.541	-0.566	- 10
	-0.656	-0.754	0.0	115
c6	-0.544	-0.156	-0.824	- 82
	0.792	0.227	-0.566	- 18
	0.276	-0.961	0.0	116
c7	-0.194	0.532	-0.824	- 72
	0.282	-0.774	-0.566	- 28
	-0.949	-0.342	0.0	92

measured in the liquid state.

The tensors of C4 and C5 are equivalent tensors differing only in their orientation in the molecular plane. This is consistent with their measured isotropic shifts being equal.

All of the H-bonded carbon tensors which have been determined here are similar to those determined by others [32-37]. All tensors have their most shielded component σ_{33} perpendicular to the plane of the molecule. σ_{11} bisects the hexad angle and is parallel to the C-H bond. σ_{22} is tangent to the ring and orthogonal to the other two axes. The magnitude of σ_{33} of these tensors follows the general trend that the value of the most shielded component of the tensor decreases with increasing substitution on the aromatic ring; i.e., σ_{33} of the H-bonded carbon tensor of pentamethyl benzene is less than σ_{33} of the tensors of C3,C4,C5,C6, which in turn are less than σ_{33} of the benzene carbon tensor. In addition, σ_{33} of the tensors of C4,C5, and C6 are all approximately equal to σ_{33} of the H-bonded carbon tensors of p-xylene [35].

Although C3 and C6 are both adjacent (ortho) to fused aromatic carbons, σ_{33} of their respective tensors are quite different; their in-plane components, however, are essentially the same. Since σ_{33} of the C6 tensor equals those of the tensors of C4 and C5 it seems that the electronic structure perpendicular to the plane of the ring around C3 is perturbed to a greater extent that that around C6.

6.3.1.2 fused (non-H bonded) aromatic carbons (C2,C7)

$\bar{\sigma}$ of C2 equals the measured liquid σ_i. The orientation of this tensor is consistent with other non-H bonded aromatic carbons tensors

[32-37]: σ_{33} is perpendicular to the plane of the molecule, σ_{11} is parallel to the carbon-substituent bond and σ_{22} is tangent to the ring of the molecule.

$\bar{\sigma}$ for C7 is 3 standard deviations greater than σ_i. The orientation of σ_{22} is turned away approximately 10 degrees from the C4-C7 bond, and is closer to being parallel to the bisector of the hexad angle.

As has been observed previously, σ_{22} for non-H bonded aromatic carbon tensors are quite different from H-bonded aromatic carbon tensors. σ_{22} for C2 and C7 tensors are -47 ppm and -27 ppm respectively, in comparison to -12 ppm to -18 ppm for the H-bonded carbon tensors.

The values of the principal elements of the two tensors are quite different from one another. C7 is bonded to an aromatic ring; C2 is bonded to the methylene carbon. The orientations of the substituent bonds with respect to their respective bisector of the hexad angles are also quite different. van Dongen Torman [37], has observed that the substituted carbon tensor in acetophenone was similar to those tensors on carbons bonded to methyl groups. If substituent type does not alter the ^{13}C shift tensor, then the difference in the two tensors must come from the different orientations of the substituent bonds.

6.3.1.3 methylene carbon (C1)

As has been generally the case here, the the trace of the chemical shift of the methylene carbon tensor equals the isotropic shift. The methylene tensor has a much smaller anisotropy than the aromatic tensors. The least shielded tensor element, σ_{11} is

perpendicular to the plane of the molecule; σ_{22} bisects the H-C-H bond and lies in the plane containing the CH_2 group; σ_{33} is in the plane of the molecule, orthogonal to the other two directions and lies "along" the C-C-C bond direction.

The assignments of σ_{11},σ_{22}, and σ_{33} are consistent with other methylene tensors. The most shielded direction is in the plane approximately "along" the C-C-C bond and the least shielded is approximately perpendicular to the plane of the C-C-C bond (in this case, the perpendicular to the plane of the molecule) for eicosane [38], ammonium hydrogen malonate [39] and malonic acid [40].

The values of the principal elements and their respective orientations of this methylene tensor are approximately equal to the methylene tensor determined for "interior methylene" carbons on the long chain molecule eicosane [38]. It is symmetrically located between two identical functional groups, in this case, two benzene rings. On the other hand, relative to the values of the principal elements of the methylene carbons on ethyl benzene (σ_{11}=100, σ_{22}=103, σ_{33}=121), the values of the principal elements of the methylene carbon tensor here are all shifted down-field and have a slightly greater anisotropy. The ethyl benzene methylene carbon is, however, not symmetrically located between two identical substituents, but rather between two very different substituents. This may account for the observed differences.

6.3.2 error analysis

6.3.2.1 statistical errors

The statistical errors generated here are large in comparison to

those reported elsewhere [34,36], but are of the same order of magnitude as those recorded by Gibby [41].

The errors are relatively large because the errors in the coefficients of the rotation plots are large. In orientation 1, the errors are approximately ± 1 unit for the constant term (A) and ± 2 to 3 units for the cosine (B)and sine terms (C). In orientation 2, the errors are consistently larger: ± 2 units for the constant term, ± 3 to 4 units for the cosine and sine terms. The larger error in orientation 2 is due to the large error in measured peak positions due to the heavy overlap of peaks. A large simplification of the spectra in orientation 2 would occur if the crystal were mounted such that the magnetic field were in some symmetry plane of the crystal, e.g. the ac plane, and causing various ^{13}C tensors to become magnetically equivalent. The number of inequivalent carbons and, in consequence, the number of peaks in a spectrum could be reduced by a factor of 2. The errors in determining peak positions would then be reduced and the errors of the coefficients of the rotation plots could become comparable to those in orientation 1.

For both orientations, a larger magnetic field would help to simplify the spectra by increasing the separation of the peaks.

6.3.2.2 systematic errors

Two systematic errors are possible:

i) an error in the location of the chemical shift reference and

ii) a shift in the measured peak position caused by bulk susceptibility effects.

i) reference zero

Solid adamantane and neat methyl iodide at room temperature were used as references. Adamantane was assumed to resonate 90.5 ppm (methylene) and 100 ppm (methine) from neat liquid benzene [42]. Methyl iodide was assumed to resonate 149 ppm from neat liquid benzene [42]. Reference positions were recorded before and generally after a set of about 4 ^{13}C spectra were taken. An error in the reference zero would essentially change the constant term of the rotation plots, shifting the the resultant principal axes values by the same amount.

ii) bulk susceptibility

The measured resonant frequency of a given nucleus in a molecule depends upon the shape of the macroscopic sample through its bulk susceptibility [43]. Following the method of Vaughn [44], the crystal shape was approximated by an ellipsoid. The bulk volume susceptibility χ, as well as its anisotropy, $\Delta\chi$ are $.94 \times 10^{-6}$ and $.5 \times 10^{-6}$ respectively [45]. Using the demagnetizing factors of Osborn [46], the shift in peak positions was calculated as a function of a few rotation angles. The peaks shift by approximately +.5 to +1.5 ppm, depending upon the crystal orientation. This shift is very small in comparison to the large aromatic carbon anisotropy of ±100ppm and small in comparison to the methylene carbon anisotropy of ±15ppm. To approximate the bulk susceptibility effect on the methylene carbon tensor, the measured peak positions were all increased a uniform 1 ppm and the tensor was recalculated. Within statistical errors, the new tensor was identical with the old tensor.

Appendix O. SOLID ECHO

The two-pulse solid (dipolar) echo sequence refocuses dipolar-coupled spins a time τ after the application of the second pulse. The basic pulse sequence is:

$$90^{0}y - \tau - 90^{0}x - \tau - \text{detect} \qquad \text{AO.1}$$

The dipolar echo of a simple two spin system can be described exactly and is given here.

Let I_1 and I_2 be the two spins coupled via the dipolar interaction; i.e. in the rotating frame, the Hamiltonian is given by

$$H = A(I_1 \cdot I_2 - 3\, I_{1z} I_{2z}) \qquad \text{AO.2}$$

where A is equal to $((\gamma_{I1}\gamma_{I2}h)/2r^3)\ (3\cos^2\theta - 1)$ and θ is the angle between the magnetic field Ho and the vector connecting I_1 and I_2.

This Hamiltonian can be easily represented as a matrix:

$$A/2 \begin{array}{c} \\ |S\rangle \\ |T_+\rangle \\ |T_0\rangle \\ |T_-\rangle \end{array} \begin{array}{c} \begin{array}{cccc} |S\rangle & |T_+\rangle & |T_0\rangle & |T_-\rangle \end{array} \\ \begin{bmatrix} 0 & 0 & 0 & 0 \\ 0 & -1 & 0 & 0 \\ 0 & 0 & 2 & 0 \\ 0 & 0 & 0 & -1 \end{bmatrix} \end{array} \qquad \text{AO.3}$$

with basis vectors

$$|S\rangle = 1/\sqrt{2}\ (|+-\rangle - |-+\rangle)$$

$$|T_+\rangle = |++\rangle$$

$$|T_0\rangle = 1/\sqrt{2}\ (|+-\rangle + |-+\rangle)$$

$$|T_-\rangle = |--\rangle$$

From this point on $|S\rangle$ is ignored.

The density matrix ρ satisfies the equation

$$d\rho/dt = -i[H,\rho] \qquad \text{A0.4}$$

which has the formal solution when H is time independent,

$$\rho(t) = e^{-iHt}\ \rho(0)\ e^{iHt} \qquad \text{A0.5}$$

where $\rho(0)$ is the density matrix at time t=0.

The normalized x-component of the free induction decay in the rotating frame, assuming no relaxation, is given by

$$\langle I_x \rangle = \mathrm{Tr}[I_x \rho(t)]/\mathrm{Tr}[I_x \rho(0_+)] \qquad \text{A0.6}$$

The rest of the appendix discusses the state of the density matrix and $\langle I_x \rangle$ at various points in the dipolar echo sequence.

$\rho(0) = I_z$. The net effect of the first 90^0_y pulse is to bring the magnetization along the rotating frame x axis; i.e.

$$\rho(0_+) = e^{-iI_y\pi/2}\ I_z\ e^{iI_y\pi/2} \qquad \text{A0.7}$$
$$= I_x$$

Following this initial 90^0_y pulse, the system evolves under the influence of the interaction term H. Substituting for H and $\rho(0_+)$ in equation A0.6, $\rho(t)$ is given by

$$\rho(t) = 1/\sqrt{2} \begin{bmatrix} e^{iAt/2} & 0 & 0 \\ 0 & e^{-iAt} & 0 \\ 0 & 0 & e^{iAt/2} \end{bmatrix} \begin{bmatrix} 0 & 1 & 0 \\ 1 & 0 & 1 \\ 0 & 1 & 0 \end{bmatrix} \begin{bmatrix} e^{-iAt/2} & 0 & 0 \\ 0 & e^{iAt} & 0 \\ 0 & 0 & e^{-iAt/2} \end{bmatrix}$$

$$= 1/2 \begin{bmatrix} 0 & e^{i3At/2} & 0 \\ e^{-i3At/2} & 0 & e^{-i3At/2} \\ 0 & e^{i3At/2} & 0 \end{bmatrix} \quad \text{A0.8}$$

Substituting for $\rho(t)$ in equation A0.6

$$\langle I_x \rangle = \cos(3At/2) \quad \text{A0.9}$$

The system is unperturbed for a time t, after which a second, 90^0_x pulse is applied. Immeediately after this pulse the density matrix $\rho(t_+)$ is given by

$$\rho(t_+) = e^{-iIx\pi/2}\, \rho(t)\, e^{iIx\pi/2} \quad \text{A0.10}$$

$$\rho(t_+) = 1/\sqrt{2} \begin{bmatrix} 0 & e^{-i3At/2} & 0 \\ e^{i3At/2} & 0 & e^{i3At/2} \\ 0 & e^{-i3At/2} & 0 \end{bmatrix}$$

where

$$e^{-iIx\pi/2} = \begin{bmatrix} 1/2 & -i/2 & -1/2 \\ -i/\sqrt{2} & 0 & -i/\sqrt{2} \\ -1/2 & -i/\sqrt{2} & 1/2 \end{bmatrix} \quad \text{A0.11}$$

That is, immediately after the second 90^0 pulse

$$\rho(t_+) = \rho(-t) \quad \text{A0.12}$$

If the system is unpertubed for a time τ, it again evolves under the influence of the interaction term, H.

$$\rho(t+\tau) = e^{-iH\tau}\ \rho(t_+)\ e^{iH\tau}$$

$$= 1/\sqrt{2} \begin{bmatrix} 0 & e^{i3A(t-\tau)/2} & 0 \\ e^{-i3A(t-\tau)/2} & 0 & e^{-i3A(t-\tau)/2} \\ 0 & e^{i3A(t-\tau)/2} & 0 \end{bmatrix} \qquad \text{A0.13}$$

$\rho(t+\tau)$ has the same form as $\rho(t)$ before the 90^{o}_{x} pulse is applied, with $(t-\tau)$ substituted to t. Therefore, the magnetization is given by

$$\langle I_x \rangle = \cos(3A(t-\tau)/2) \qquad \text{A0.14}$$

For times τ=t $\langle I_x \rangle$ = 1, the initial magnetization.

Appendix 1. NICOLET 293 PATCH PANEL CONNECTIONS

The Nicolet 293 timer patch panel connections are shown in figures A1.1 and A1.3. The patch panel connections are essentially the same for the two experiments: the ONP experiment contains one additional input to the OR gate which goes to the pulse sorter. The timers are connected to different outputs in the two experiments. Figure A1.2 and A1.4 depict the resultant pulse sequences. Typical times are also listed.

The figures follow the convention of preceeding connections in patch panel A with the letter A; connections in panel B are not preceeded with the letter B. Timer outputs are located at AA1 through AA10. Output connections are labelled for the two experiments.

Nine inverting buffers are located on panel A; inputs are located at AH1 through AH9; outputs, AG1 through AG9. Ten one shots are also located on panel A; inputs are located at AF1 through AF10; outputs at AI1 through AI10. The first seven one shots trigger on the rising edge of the trigger pulse; the last three one shots trigger on the falling edge.

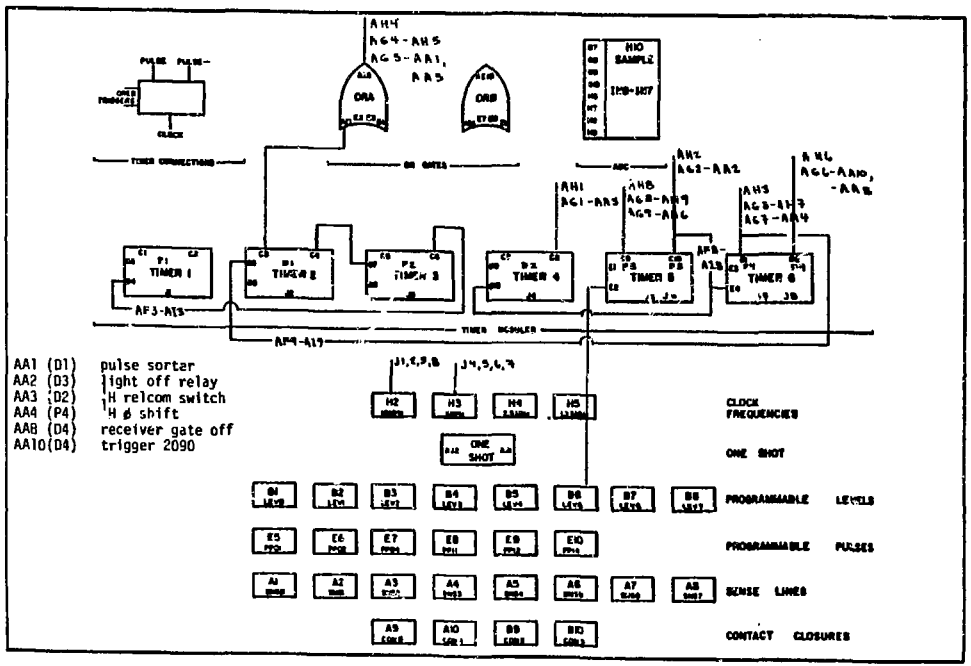

GENERAL PURPOSE CONTROLLER
PATCH PANEL DIAGRAM
NICOLET 293

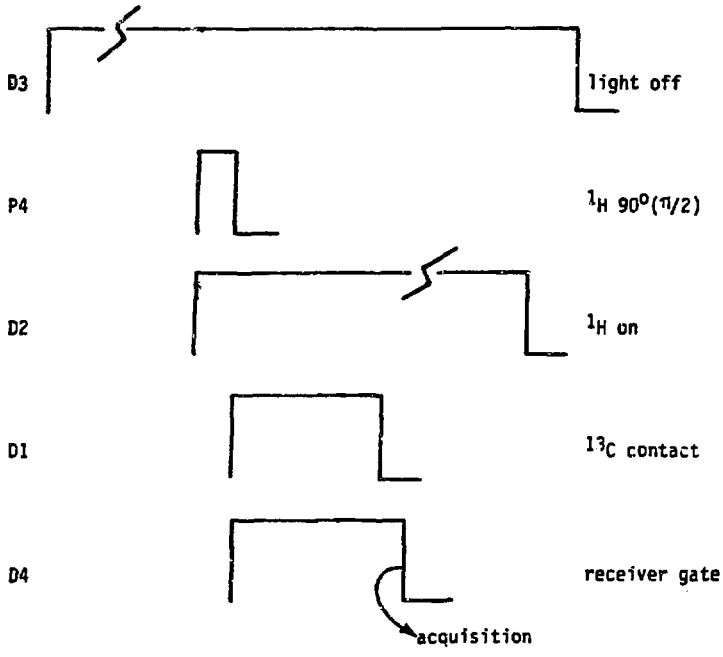

P4 = 4.5 us
D2 = 400 ms
D1 = 5 ms
D4 = 5 ms + 200 us

D3 (light off) 5 s

typical times PENIS experiment

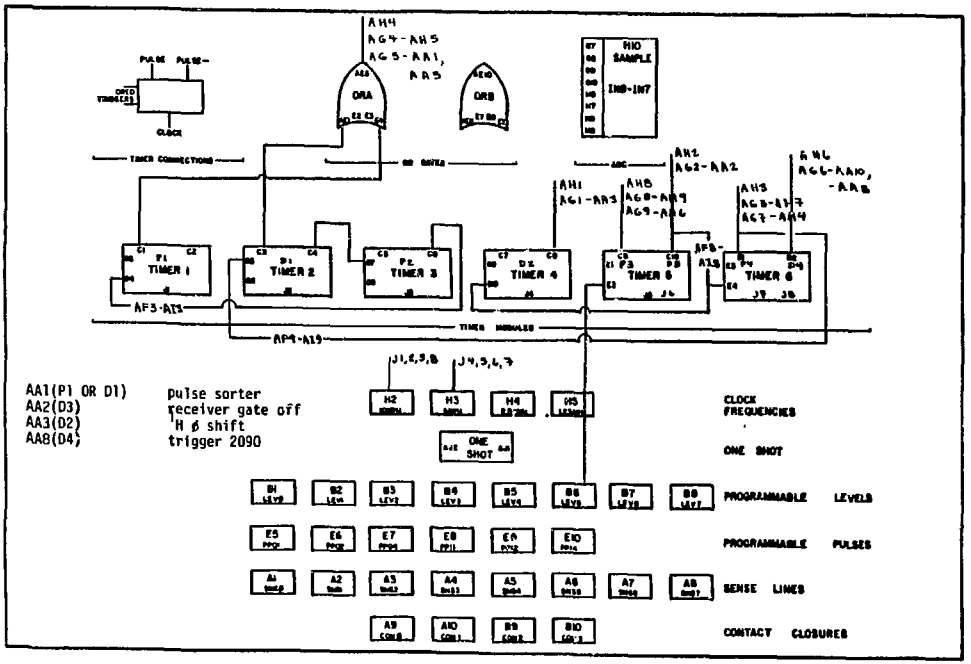

GENERAL PURPOSE CONTROLLER
PATCH PANEL DIAGRAM
NICOLET 293

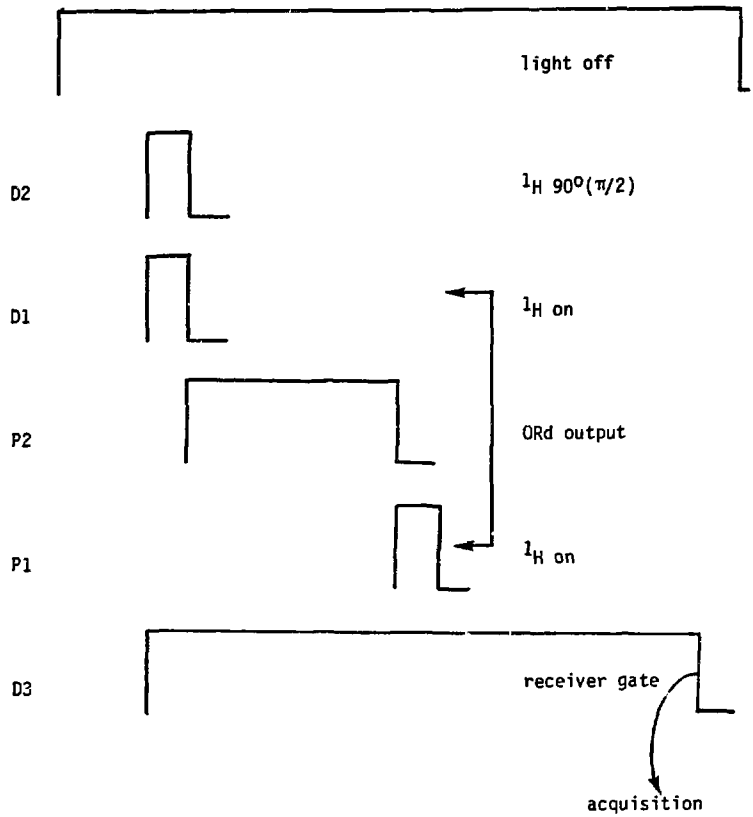

D1, P1 = 2.5 us
D2 = 2.5 us
P2 = 20 us
D3 = 45 us

typical times ONP experiment

light off 5 s

Appendix 2. MODIFICATIONS OF NTCFT

A2.1 Patch for 2090/201

The modifications to NTCFT #1002 which allow data acquisition through the transient recorder 2090/201 are listed on the following page. Program changes were accomplished using Nicolet's HIBUG program. The format used is

address/old instruction ---->new instruction

The assembler mnemonic and/or a description of the instruction is included.

The modifications can be divided into three parts:

i)change of ADC control word

ii)changes to make 2090/201 and Nic-80 data collection compatible

iii)changes to allow data acquistion <20 μs after start of rf pulses.

The IPLS experiment must be used. The total length of time from the start of the rf pulses to the start of data acquistion must be > 20 μs. This last requirement insures that the Nic-80 is in measure mode before it is triggered.

```
*LOA NTCCON 5640
*RUN HIBUG

6151/0000026 ----> 0100026    /set cword (bit 15 high)
7600G

*STO NTCCON 5620-7577;7500:P


*LOA NTCEXC
*RUN HIBUG

 637/0005001 ----> 0005000            interface to transient recorder
 134/3103427 ---->     136
7600G

*STO NTCEXC 0-1777:P


*LOA NTCDIN 2000
*RUN HIBUG

4133/0111777 ----> 2111470
5470/0000000 ---->  101777
                             /to maintain bit 15 of cword when cword
                             /gets reset
4041/0111776 ----> 2111471
5471/0000000 ---->  101776

4721/2505543 ----> 2125543    /MPOM POINT1
4724/2505544 ----> 2125544    /MPOM POINT2
4735/2125544 ---->    1472    /JMP 5472
5472/0000000 ----> 2125544
5473/0000000 ----> 2125544              to acquire data <20µs
5474/0000000 ----> 2125543              after start of rf pulses
5475/0000000 ---->     736    /JMP to 4736
5065/0005001 ---->    5000
5272/3111562 ---->    1272    /JMP to 5272

4244/2111733 ---->     347    /JMP to 347
4452/3001451 ---->     453    /JMP to 453
4463/3001452 ---->     464    /JMP to 464
5314/0110304 ---->    1272    /JMP to 5272 (JMP TO <RUNSTEM)

7600G

*STO NTCDIN 2000-5617;7600
*LOA NTCDIN 110000-113617;7600:P
*STO NTCDIN 110000-113617;7600:P
```

A2.2 Patch for multiple contact PENIS

Modifications to NTCFT #1002 to allow mutiple contacts in the PENIS experiment are shown in Table A2.1. Nicolet's HIBUG program was used; format for changes are as shown below

address/instruction /mnemonic

Changes for the multiple contact experiment can be divided into three parts:

i) create new command=NC

ii) initialize for counting number of contacts

iii) determine number contacts left to do, retrigger rf pulses if not equal to zero.

The number of contacts are entered using the command 'NC'. E7 (PP04) on the Nicolet 293 patch panel retriggers the contact/mix PENIS pulse.

```
*LOA NTCDIN
*RUN HIBUG

2776/2707066     /MMOMZ
2777/   1003     /JMP (to 4003)
3000/3111005     /MEMA @ PNCON
3001/2405006     /ACCM NCODO
3002/1001007     /JMP @ PGOR1
3003/   4204     /PP04
3004/1001010     /JMP @ PGOR4
3005/   6151     /PNCON
3006/      0     /NCDO
3007/   4406     /PGOR1
3010/   4541     /PGOR4

3011/      0     /INI
3012/3111005     /MEMA @ PNCON
3013/2405006     /ACCM NCODO
3014/1001011     /JMP @ INI

4124/3000126     /JMS @ FLG
4125/    133     /JMP (to 4133)
4126/   3011     /FLG

5017/1001465     /JMP @ BADSET

5075/      0     /NC
5076/3001447     /JMS @ YFIN
5077/   6152     /YFIN

5520/316303      /(n=316,c=303)

7600G

*STO NTCDIN 2000-5617;7600
*LOA NTCDIN 110000-113617;7600:P

*STO NTCDIN 110000-113617;7600:P
```

A2.3 Patch for second variable timer

Table A2.3 lists the changes to NTCFT which create a second variable timer. Changes to NTCPAR allow input of variable times. Changes to NTCDIN implement the variable times during run time.

A second variable timer was necessary when varying the contact/mix time in the PENIS experiment. NTCFT has only on variable timer (D1) which was used to vary the contact/mix pulse. The second timer was used as the receiver gate=contact/mix + 1 dwell time.

Variable times are entered with the command 'CD' (CCD on). D3 is the variable timer; the list is terminated with the entry 0.

```
*LOA NTCDIN 2000
*RUN HIBUG

4215/      1
4217/2405728      /ACCM YD3
4220/3001457      /JMS @ TWI04
4221/   5273      /YD3
4222/    346      /JMP 346
7600G

*STO NTCDIN 2000-5617;7600
*LOA NTCDIN 110000-113617;7600
*STO NTCDIN 110000-113617;7600:P


*LOA NTCPAR
*RUN HIBUG

4154/3025204      /ONEM @ UFLAG4
4155/    156      /JMP 156
4161/3001206      /JMS @ TWI04
4164/ 545160      /EXCT POAC
4170/3024162      /ONEM @ POINTC
7600G

*STO NTCPAR 2000-5617;7600
*LOA NTCPAR 104000-107617;7600
*STO NTCPAR 104000-107617;7600:P
```

Appendix 3. DATA TRANSFER FROM NIC-80 TO VAX/VMS 11/780

Data collected on the Nic-80 was transferred to the VAX/VMS 11/780. The purpose of the data transfer was

i) for archival storage of data on magnetic tape.

ii) for efficient plotting of all fourier transformed files

iii) for efficient determination of peak position in ^{13}C spectra.

Data was transferred to the VAX using the command 'U2'. The necessary program changes to NTCFT #1002 are shown in Table A3.1. The 'U2' command can be used in the standard Nicolet link ('LI' command). A fortran program is simultaneously run on the VAX and listed on the succeeding pages. Both programs are based on programs by W.Shih[21] and J.McCracken.

The Nic-80 is connected to the VAX via an RS232 bus. Communication lines operate in normal mode, with the baud rate set to 2400. For a more extensive description of various parts of the programs, see W.Shih [21].

```
*LOA NTCUSR 2000
*RUN HIBUG

5176/0000000        /VAXOUT
5200/2001227        /JMS XMIT
5201/2001220        /JMS RXON   LOOP0
5202/2165304        /ZERM START
5203/2001261        /JMS STATRD
5204/2001220        /JMS RXON    LOOP1
5205/3111303        /MEMA @ TEMP
5206/2001227        /JMS XMIT
5207/3111303        /MEMA @ TEMP
5210/2505304        /A+MM START
5211/2125303        /MPOM TEMP
5212/2707302        /MMONZ SIZE
5213/   1204        /JMP LOOP1
5214/2001220        /JMS RXON
5215/2111304        /MEMA START
5216/2001227        /JMS XMIT
5217/1001176        /JMS LOOP0

5220/      0        /RXON
5221/   6554        /RSINF       LOOP2
5222/   1221        /JMP LOOP2
5223/  44563        /RSIN
5224/ 472021        /A-MAZ (021
5525/   1221        /JMP LOOP2
5526/1001220        /JMP @ RXON

5527/      0        /XMIT
5230/2405305        /ACCM CHECKSUM
5231/2001250        /JMS RSXMIT
5232/2111305        /MEMA CHECKSUM
5233/ 405025        /RISH 25
5234/2001250        /JMS RSXMIT
5235/2111305        /MEMA CHECKSUM
5236/ 405032        /RISH 32
5237/2001250        /JMS RSXMIT
5240/2111305        /MEMA CHECKSUM
5241/ 404037        /RISH 37
5242/2001250        /JMS RSXMIT
5243/ 110015        /MEMA (015    (CARRIAGE RETURN)
5244/   6574        /RSOUTF      LOOP3
5245/   1244        /JMP LOOP3
5246/   4573        /RSOUT
5247/1001227        /JMP @ XMIT

5250/      0        /RSXMIT
5251/  10037        /AND (37
5252/   4354        /TACMQ
5253/ 110040        /MEMA (40
5254/   4341        /OR
```

```
5255/   6574        /RSOUTF      LOOP4
5256/   1255        /JMP LOOP4
5257/   4573        /RSOUT
5260/10[illegible]250        /JMP @ RSXMIT

5261/      0        /STATRD
5262/  44034        /STATUS
5263/   5012        /LASH 12
5264/2011300        /ANDA MASK1
5265/2511277        /A+MA DSTART
5266/2405304        /ACCM START
5267/  44034        /STATUS
5270/   5046        /LLSH 6
5271/ 210000        /ACPA
5272/2013300        /ANDAZ MASK1
5273/ 162000        /ZERZ
5274/2111301        /MEMA K16K
5275/2405302        /ACCM SIZE
5276/1001261        /JMP @ STATRD

5277/ 100000        /DSTART
5300/  36000        /MASK1
5301/  40000        /K16K
5302/      0        /SIZE
5303/      0        /TEMP
5304/      0        /START
5305/      0        /CHECKSUM

5306/      0        /XON
5307/ 110026        /MEMA (026
5310/2001227        /JMS XMIT
5311/1001306        /JMS @ XON

5523/   5176        /VAXOUT

7600G


*STO NTCUSR 2000-5617:P
```

```
C
C  This routine receives data from the nic-50 via rs232.  nic
C  sets 32 bit word transmitter as a string of 5 bits,byte, 4
C  bytes/word followed by a carriage return.  format 001xxxxx
C  where xxxxx are significat bits.  001 insures no control
C  characters.  program to be used with u2 command of ctrl 1002.
C  u2 can be used in link (li).  strictly data transferred, not
C  parameter table.  parameters entered at terminal;
C  output file is title 1:4 + no.; e.g. for title 'peris' output
C  files (if in link) are peni01.dat,peni02.dat,etc.
C  basic unpackwire routine by w.shih.
C
C       A(*)        DATA POINT ARRAY
C       CHECKSUM    RUNNING CHECKSUM CALCULATED DURING DATA RECEIVE
C       TITLE       ASCII HEADER BLOCK WRITTEN ON OUTPUT FILE
C       fname1      title 1:4 (used for output file name)
C       MASK1       00011111 MASK USED TO SELECT 5 LSB OF EACH BYTE
C       MASK2       11111111111111111111 MASK USED TO SELECT
C                   20 LSBs OF EACH 32 BIT WORD ON VAX
C       XX          SET TO OCTAL 21 FOR CTRL-Q TO INITIATE
C                   DATA TRANSMISSION
C       K1          'x' from nic-50 to start receiving data
C       ANS         total number of spectra to be sent
C       IP          NUMBER OF DATA POINTS
C       IJ(*)       VECTOR USED FOR DATA REAL-IN, 4 WORDS LONG,
C                   ONE BYTE PER LOCATION
C       ISUM        RUNNING SUM USED IN PACKING DATA
C
0001          DIMENSION A(15736),ST(2),IJ(4),DATE(10)
0002          INTEGER A,CHECKSUM,ANS,DATE,PA,ivp,ifatten
0003          REAL MA,MF,DT
0004          CHARACTER ST
0005          character*4 fname1
0006          CHARACTER*6 fname
0007          CHARACTER*60 TITLE
0008          LOGICAL CONTIN,COUNT,TYPE,IOS
0009          integer*4 OTSSCVT_L_TI,SYSSGETMSG
0010          character sys*sg*132
0011          integer*2 buf
0012          character*2 ch1
C
C
0013          OPEN (UNIT=01,NAME='FOR001',TYPE='OLD')
0014          OPEN (UNIT=02,NAME='FOR002',TYPE='NEW',
              1FORM='UNFORMATTED')
0015          CONTIN = .TRUE.
0016          COUNT = .FALSE.
0017          TYPE = .FALSE.
0018          IOS = .FALSE.
0019          MAXLIM = 100
C  SUPPRESS ERROR MESSAGES FROM INTEGER OVERFLOW
C  CAUSED BY CHECKSUM CALCULATION
001A          CALL ERRSET(70,CONTIN,COUNT,TYPE,IOS,MAXLIM)
001I          MASK1 = "37
001J          MASK2 = "3777777
```

```
0025            KK = 21
0026      910   write (6,901)
0025      901   format('$enter number of spectra  ')
0028            read(5,*)nns
0027      1000  WRITE (6,1100)
0028     1100   FORMAT('$ENTER POINTS PER FILE  ')
0029            READ(5,*)IP
0030            WRITE(5,403)
0031      403   FORMAT('$ENTER THE DATE(10A1)  ')
0032            READ(5,404)DATE
0033      404   FORMAT(10A1)
0034      100   WRITE(5,560)
0035      560   FORMAT('0frequency width, THE # OF PASSES,
                1   spec freq, diameters
                2   freqs (order 3,2)FORMAT(f5.2,15,3f10.5)')
0036            READ(5,*)FP,PA,sf,adam1,adam2
0037      501   FORMAT(f5.2,15,3f10.5)
0038            WRITE(5,590)
0039      590   FORMAT('0ENTER vp or 2000 and if atten--
                1   format(215)')
0040            READ(5,*)ivp,ifatter
0041      591   FORMAT(215)
          c
          C     SET TITLE AND OPEN FILE
0042      195   WRITE(6,910)
0043      910   FORMAT('0ENTER TITLE(A60),FILENAME IS
                1   FIRST 4 CHAR incremented ')
0044            READ(5,911)TITLE
0045      911   FORMAT(A50)
          c
0046      611   WRITE(6,620)
0047      620   FORMAT('0WHEN READY TO RECEIVE TYPE GO ON THE VAX')
0048            READ(5,525)ST
0049      525   FORMAT(2A1)
0050            IF(ST(1).EQ.'g')GO TO 630
0051            GO TO 611
0052      630   CONTINUE
          c
          c     start of do loop to transmit nns spectra
          c
0053            do 999 jmit=1,nns
0054            ic=jmit
0055            ISTAT=OTSSCVT_I_TI(IC,CHI,%VAL(2))
0056            Jmes=SYSSGET*SG(%VAL(ISTAT),
                1   *SGLEN,SYSMSG,%VAL(-1),)
0057            IF(ISTAT.NE.1)WRITE(6,99)SYSMSG(1:MSGLEN)
0058      99    FORMAT(1X,A)
0059            fname1=title(1:4)
0060            frame=fname1//ch1
0061            open(unit=89,name=fname,type='new',
                1   carriagecontrol='list')
          C     FILL IN PARAMETER TABLE
0062            WRITE(9,911)frame
0063            WRITE(9,404)DATE
0064            WRITE(9,405)ISPEC,IP
0065            WRITE(9,591)ivp, ifatter
0066            WRITE(9,501)FP,PA,sf,adam1,adam2
```

```
0067      405   FORMAT(2I5)

          c
          c
          C       NOW LOOP OVER THE NUMBER OF POINTS, RECEIVING AND
          C       PACKING THEM ONE AT A TIME.  EACH TIME THE VAX IS
          C       READY FOR A NEW WORD A CONTROL-Q COMMAND IS ISSUED TO
          C       THE NIC-80. UPON RECEIVING
          C       A CONTRL-Q THE NIC OUTPUTS ONE WORD
          c       write ^q to start transmission
          c       wait for ^v from nic80 to signal ready to send data
          C
0068      802   read (1,998) n,(ij(i),i=1,n)
0069      998   format(q,<n>a1)
0070            isum=0
0071            do 955 i=4,1,-1
0072            ij(i)=iand(ij(i),mask1)
0073            ishift=(i-1)*5
0074      955   isum=ior(isum,ishft(ij(i),ishift))
0075            k1=iand(isum, mask2)
0076            write(5,955)k1
0077      966   format('$received k1=',o20)
0078            if (kk.eq.'25') then
0079                    write (2) kk
0080                    checksum=0
0081                    write(5,977)
0082      977           format('$received k1, sent ^21')
0083            else
0084                     go to 802
0085            end if
          c
          C  FOR EACH FILE, LOOP THROUGH IP TIMES TO RECONSTRUCT
          C  IP WORDS FROM IP*4 BYTES.  A 20 BIT WORD IS RECEIVED
          C  IN THE FOLLOWING BYTE SEQUENCE:
          C
          C       AC4-3,AC3-5,AC14-10,AC15-15 <CR>
          C
          C     RECONSTRUCTION (PACKING) OCCURS BY APPROPRIATE
          C     LEFT-SHIFTING AND LOGICAL OR-ING OF THE FOUR
          C     BYTES STORED IN IJ(*)
          C
0086            IPP=IP+1
0087            DO 200, K=1,IP
0088            WRITE (2) KK
0089      100   READ (1,1000) N,(IJ(I),I=1,N)
0090      1000  FORMAT (Q,<N>A1)
0091            ISUM = 0
0092            DO 122 L=4,1,-1
0093            IJ(L) = IAND(IJ(L),MASK1)
0094            ISHIFT = (L-1)*5
0095      122   ISUM = IOR(ISUM,ISHFT(IJ(L),LSHIFT))
0096            CHECKSUM = CHECKSUM + ISUM
0097            A(K) = ISUM
0098        200 CONTINUE
          C  NOW RECEIVE AND RECONSTRUCT THE CHECKSUM
          C     CALCULATED BY THE 1190,
          C     AND COMPARE TO THE LOCALLY CALCULATED ONE.
```

```
      WRITE (2) KK
      READ(1,1000) N,(IJ(I),I=1,N)
      ISUM = 0
      DO 220, I=4,1,-1
      IJ(L) = IAND(IJ(L),MASK1)
      ISHIFT = (L-1)*8
220   ISUM = IOR(ISUM,ISHFT(IJ(L),ISHIFT))
      CHECKSUM = IAND(CHECKSUM,MASK2)
      ISUM = IAND(ISUM,MASK2)
      WRITE(6,1010) fname,CHECKSUM,ISUM
1010  FORMAT('0FILE =',a5/'0CALCULATED CHECKSUM =',O9/
     1  '0RECEIVED CHECKSUM =',O9)
C     CHECK FOR NEGATIVE NUMBERS
      KKK=2000000
      DO 21 I=1,IP
         IF(A(I).LT.KKK)GO TO 21
         A(I)=A(I)-3777777
   21    CONTINUE
C     NOW OUTPUT NUMBERS
      WRITE(8,2000)(A(I),I=1,IP)
2000  FORMAT (8I10)
999   continue
      write(5,905)
905   format('$another set of files? (y/n;')
      read(5,906)ans
906   format(a1)
      if(ans.eq.'y')go to 910
      END
```

PROGRAM SECTIONS

	Name	Bytes	Attributes
0	$CODE	1713	PIC CON REL LCL SHR EXE RD NOWRT LONG
1	$DATA	555	PIC CON REL LCL SHR NOEXE RD NOWRT LONG
2	$LOCAL	67595	PIC CON REL LCL NOSER NOEXE RD WRT LONG

ENTRY POINTS

Address	Type	Name
0-00004000		XMIT$SMAIN

VARIABLES

Address	Type	Name	Address	Type	Name
2-20010598	R*4	ADAM1	2-0001065C	R*4	ADAM2
2-20010622	I*4	CHFCISU*	2-00010564	CHAR	CHI
2-20010644	R*4	IT	2-00010588	CHAR	FNAME
2-20010668	I*4	I	2-00010614	I*4	IC
2-20010712	I*4	IPP	2-00010584	I*4	ISPEC
2-20010694	I*4	IVP	2-0001065C	I*4	JMES
2-200106C4	I*4	KK	2-00010718	I*4	KKK
2-20010584	L*4	LOJ	2-00010704	I*4	LSHIFT
2-200106C8	I*4	MASK2	2-00010638	I*4	MAXLIM
2-20010658	I*4	N	2-0001060C	I*4	NNS
2-20010570	CHAR	STSMS3	2-00010504	CHAR	TITLE

Address	Type	Name	Address	Type	Name
2-20010538	I*4	ANS	2-00010695	I*2	#CF
2-20010685	L*4	CONTIN	2-00010584	L*4	COUNT
2-20010584	CHAR	FNAME1	2-00010600	R*4	FP
2-20010598	I*4	IPATTEN	2-00010500	I*4	IP
2-20010618	I*4	ISTAT	2-00010704	I*4	ISUM
2-20010612	I*4	JMIT	2-00010714	I*4	K
2-20010730	I*4	KL	2-00010704	I*4	L
2-20010630	R*4	MA	2-00010530	I*4	MASK1
2-20010580	R*4	MF	2-00010600	I*4	MSGLEN
2-20010590	I*4	PP	2-00010504	R*4	SF
2-20010680	I*4	TYPE			

ARRAYS

Address	Type	Name	Bytes	Dimensions
2-00000000	I*4	A	65944	(16738)
2-20010590	I*4	DATE	40	(10)
2-20010580	I*4	II	16	(4)
2-20010588	CHAR	ST	2	(2)

Appendix 4. ONP calculation programs

This appendix contains a listing of the computer program used to calculate the theoretical curves of figure 3.5. The flow chart of figure A4.1 describes both the control program, NEWONP, and the program which does the actual intensity vs field strength calculation, ONPOL. PLONP is a routine which plots the output of ONPOL. It is based on a subroutine by D.Goodin and is not reproduced here. Subroutines VCVTCH,EIGCH,LINV1F,and VMULFF are all IMSL subroutines which (respectively), converts a Hermitian matrix to a full complex storage mode matrix, diagonalizes a Hermitian matrix, inverts a matrix, multiplies two matrices.

Definition of input values:

D,E as defined by equation 3.8 are elements of the electron dipolar interaction tensor.

gama=γ as given in equation 3.8 is the gyromagnetic ratio of the proton spin.

A is the hyperfine interaction tensor.

p_m m=x,y,z is the relative population rate into the mth triplet state (normalized to one triplet state).

k_m m=x,y,z is the relative decay rate from the mth triplte state (normalized to one triplet).

$w_{m,n}$ m,n = x,y,zis the spin lattice relaxation rate between the mth and nth triplet states.

Typical values:

D = 395 MHz, E = 15.3 MHz

gama = 4.257E-07

A_{xx} = -29 MHz, A_{yy} = -9.2 MHz, A_{zz} = -19.0 MHz

$k_x = k_y = k_z = .333$

$p_x = .9$, $p_y = .05$, $p_z = .05$

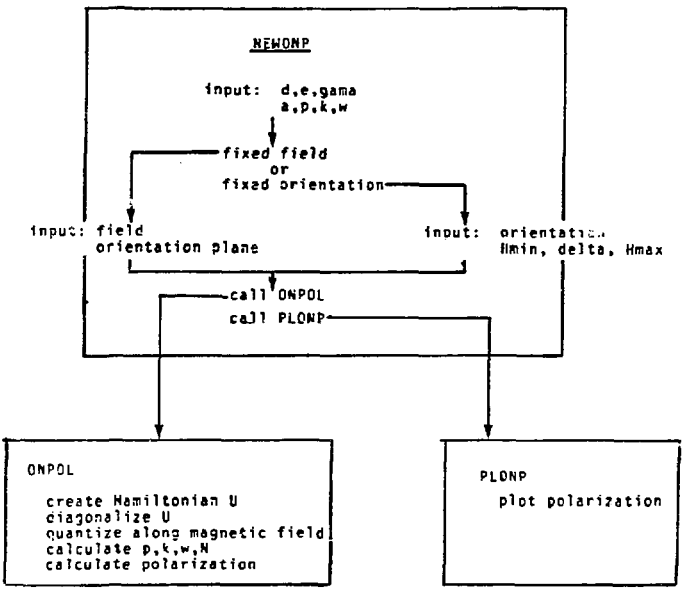
NEWONP
input: d,e,gama
a,p,k,w
fixed field
or
fixed orientation
input: field
orientation plane
input: orientation
Hmin, delta, Hmax
call ONPOL
call PLONP
ONPOL
create Hamiltonian U
diagonalize U
quantize along magnetic field
calculate p,t,w,N
calculate polarization
PLONP
plot polarization

```
0001            program newcmp
                c
                c
0002            real xp(100),yp(100),kx,ky,kz
0003            common/cnst/i,e,gama,
                1           /rates/kx,ky,kz,px,py,pz,
                2           /hyper/ax,ay,az,
                3           /relax/wxy,wxz,wyz
                c
0004            open(unit=9,status='new',name='given')
0005            call grstrt(4014,2)
0006            open(unit=8,status='old',name='input',readonly)
0007            read(8,*)i,e,gama
0008            read(8,*)kx,ky,kz,px,py,pz
0009            read(8,*)ax,ay,az
0010            read(8,*)wxy,wxz,wyz
0011            close(unit=8,status='keep')
                c
0012    999     continue
                c
0013            write(6,103)
0014    103     format(' decay and population rates=')
0015            WRITE (6,*) KX,KY,KZ,PX,PY,PZ
0016            write(6,203)
0017    203     format(/'hyperfine constants and relaxation rates')
0018            WRITE (6,*) AX,AY,AZ,WXY,WXZ,WYZ
                c
0019            write(5,333)
0020    333     format(' change 2,p=1,k=2,a=3,w=4')
0021            read(5,*)ich
0022            if (ich.EQ.1) then
0023                    read(5,*)px,py,pz
0024            else if (ich.EQ.2) then
0025                    read(5,*)kx,ky,kz
0026            else if (ich.EQ.3) then
0027                    read(5,*)ax,ay,az
0028            else if (ich.EQ.4) then
0029                    read(5,*)wxy,wxz,wyz
0030            else
0031                    continue
0032            end if
                c
0033    999     continue
                c
0034            write(6,501)
0035    501     format(' fixed field=1 or fixed orientation=2?')
0036            read(5,*)ifo
0037            if (ifo .EQ. 2) then
0038                    write(5,303)
0039    303             format(' enter theta, phi:  90,0 then y=1'/,
                1           ' 90,90 then y=1'/,
                2           ' 0,0   then z=1'/,
                3           ' xy plane is 90,angle'/,
                4           ' yz plane is angle,90'/,
                5           ' xz plane is angle,0')
                c
0040                    read(5,*)theta,phi
```

```
      c
0041                  write(5,100)
0042    100           FORMAT(' ENTER NUMBER OF FIELD POSITIONS')
0043                  read(5,*)NFLD
0044                  write(6,10)
0045     10           FORMAT(' ENTER RMIN,DELTA')
0046                  read(5,*)RMIN,DELTA
      c
0047                  DO IIK =1,NFLD
0048                  R = RMIN + delta*iik
0049                  write(6,*)R
0050                  call onpol(theta,phi,R,pol)
0051                  yp(iik) = pol
0052                  xp(iik) = R
0053                  end do
0054                  write(5,444)
0055    444           format(' new plot?')
0056                  read(5,777)ans2
0057    777           format(a1)
0058                  if (ans2.EQ.'y') then
0059                        iopt = 1
0060                  else
0061                        iopt = 0
0062                  end if
0063                  call plotp(xp,yp,nfld,iopt)
0064            else if (ifp.EQ.1) then
0065                  write(5,702)
0066    702           format(' enter field')
0067                  read(5,*)R
0068                  write(5,701)
0069    701           format(' enter if xy plane=1,yz plane=2,xz plane=3')
0070                  read(5,*)ipln
0071                  im=0
0072                  if (ipln.EQ.2) then
0073                        phi = -90.
0074                        do iik=-50,0,5
0075                        im=im+1
0076                        theta = iik
0077                        call onpol(theta,phi,R,pol)
0078                        yp(im)=pol
0079                        xp(im)=theta
0080                        end do
0081                        phi = 90.
0082                        do iik=5.90,5
0083                        im=im+1
0084                        theta = iik
0085                        call onpol(theta,phi,R,pol)
0086                        yp(im)=pol
0087                        xp(im)=theta
0088                        end do
0089                        write(6,444)
0090                        read(5,777)ans2
0091                        if (ans2.EQ.'y') then
0092                              iopt = 1
0093                        else
0094                              iopt = 0
0095                        end if
```

```
                        call plorp(xp,yp,37,iopt)
                else if(iplr.EQ.1) then
                        theta = 90.
                        do 11k=-90,90,5
                        in=in+1
                        phi = 11k
                        call onpol(theta,phi,n,pol)
                        yp(in)=pol
                        xp(in)=phi
                        end do
                        write(6,444)
                        read(5,777)an2
                        if (an2.EQ.'y') then
                                iopt = 1
                        else
                                iopt = 0
                        end if
                        call plorp(xp,yp,37,iopt)
                else if (iplr.EQ.3) then
                        phi = 0.0
                        do 11k=-90,0,5
                        theta = 11k
                        in=in+1
                        call onpol(theta,phi,n,pol)
                        yp(in)=pol
                        xp(in)= theta
                        end do
                        phi=180.
                        do 11k=5,90,5
                        theta = 11k
                        in=in+1
                        call onpol(theta,phi,n,pol)
                        yp(in)=pol
                        xp(in)= theta
                        end do
                        write(6,444)
                        read(5,777)an2
                        if (an2.EQ.'y') then
                                iopt = 1
                        else
                                iopt = 0
                        end if
                        call plorp(xp,yp,37,iopt)
                end if
        else
                go to 999
        end if
c
        write(6,555)
555     format(' continue at new orientation field=1',
     1          ' continue with new constants=2')
        read(5,*)ian
        if (ian.EQ.1) then
                go to 333
        else if (ian.EQ.2) then
                go to 999
        else
                continue
        end if
c
        call exstop
        close(unit=9,status='keep')
        end
```

VARIABLES

Address	Type	Name	Address	Type	Name
2-0000[illegible]348	R*4	AN2	5-[illegible]3000	R*4	AI
3-00000000	R*4	D	2-00000338	R*4	DELTA
2-00000340	R*4	E	2-0000[illegible]334	R*4	EMIN
2-[illegible]324	I*4	IFO	2-[illegible]33C	I*4	IIK
2-00000350	I*4	IPIN	4-00000000	R*4	KK
2-[illegible]330	I*4	NFLD	2-00000320	R*4	PHI
4-[illegible]018	R*4	PI	4-[illegible]014	R*4	PZ
6-00000004	R*4	WXZ	6-00000008	R*4	WYZ

Address	Type	Name	Address	Type	Name
5-00000004	R*4	AI	5-[illegible]	R*4	AZ
3-00000004	R*4	I	3-00000008	R*4	GAMA
2-[illegible]350	I*4	IAN	2-[illegible]320	I*4	ICH
2-[illegible]354	I*4	IN	2-[illegible]34C	I*4	LOPT
4-00000004	R*4	KY	4-[illegible]	R*4	KZ
2-[illegible]344	R*4	POL	4-[illegible]	R*4	PA
2-00000328	R*4	THETA	6-[illegible]	R*4	WXY

ARRAYS

Address	Type	Name	Bytes	Dimensions
2-00000000	R*4	IP	400	(100)
2-00000190	R*4	IP	400	(100)

```
      C
      C THIS PROGRAM FOR RUNNING ON VAX:FIELD DEPENDENCE ONP
      C
0001          subroutine ONPOL(theta,phi,h,pol)
      c
0002          common/cnst/i,e,gama
     1                /rates/kx,ky,kz,px,py,pz
     2                /hyper/ax,ay,az
     3                /relax/wxy,wxz,wyz
      c
0003          character er1,er2
0004          dimension dX1 (1000),dIJIN (5,5)
0005          COMPLEX Z(6,6),EVEC(6),WR(2000)
0006          dimension TOTS(6,2),SUMX(6),DIFK(6),CALK(6),ZZ(6,6,
0007            dimension SOMZ(6),SNORM(6),S(6)
0008            dimension AA(6,6),AAA(6,6)
0009            COMPLEX UU(6,6),SOR,ZERO2
0010          REAL KX,KY,KZ
0011          REAL E(6)
0012          COMPLEX U(6,6)
0013          dimension S(6)
0014          dimension W(6,6),WIJ(6,6),CALW(6,6)
0015            dimension TOTP(6),P(6),CALP(6)
      c
0016          BETA = 1.4
0017          GXX = 2.0003
0018          GYY = 2.0003
0019          GZZ = 2.0003
      c
0020            conv = 2.0*3.1415/360.
0021            rtheta = theta * conv
0022            rphi = phi *conv
0023            t = sin(rtheta)*cos(rphi
0024            q = sin(rtheta)*sin(rphi)
0025            r = cos(rtheta)
      c
0026          HX = T*H
0027          HY = Q * H
0028          HZ = R * H
      c
0029          ZGZ = GZZ * BETA * HZ
0030          ZGX = GXX * BETA * HX
0031          ZGY = GYY * BETA * HY
0032            ZERO1 = .5 * GAMA * HZ
0033          ZERO2 = .5 * GAMA * (HX-(0.0,1.0)*HY)
      c
0034            TR = -54.0 * 3.1416/180.0
0035            TRCOS = COS(TR)
0036            TRSIN = SIN(TR)
0037            AXX = AX
0038            AYY = AY*((TRCOS)**2)+ AZ*((TRSIN)**2)
0039            AZZ = AY * ((TRSIN)**2) + AZ * ((TRCOS)**2)
0040            AZY = (AZ-AY)*TRCOS*TRSIN
      c
      C       ENTER MATRIX HAMILTONIAN
      c
0041          U(1,1) = D - E - ZERO1
```

```
0042          U(1,2) = -(0.0,1.0)*(0.5*AZZ +ZGZ)
0043          U(1,3) = (0.0,1.0)*(ZGI + .5*AZY)
0044          U(1,4) = -ZEND2
0045          U(1,5) = -0.5*AZY
0046          U(1,6) = .5 * AYY
0047          U(2,2) = D+E - ZEND1
0048          U(2,3) = -(0.0,1.0)*ZGX
0049          U(2,4) = 0.5*AZY
0050          U(2,5) = - ZEND2
0051          U(2,6) = -(0.0,1.0)*(0.5*AXY)
0052          U(3,3) = -ZEND1
0053          U(3,4) = - (.5 * AYY)
0054          U(3,5) = (0.0,1.0)*(0.5*AXY)
0055          U(3,6) =-ZEND2
0056          U(4,4) = D-E + ZEND1
0057          U(4,5) = (0.0,1.0)*(0.5*AZZ -ZGZ)
0058          U(4,6) = (0.0,1.0)*(ZGY - 0.5*AZY)
0059          U(5,5) = D+E + ZEND1
0060          U(5,6) = -(0.0,1.0) *ZGX
0061          U(6,6) = ZEND1
0062          DO 11 I = 1,6
0063          DO 21 J = 1,6
0064          IF(I.GE.J) GO TO 21
0065          U(J,I) = CONJG(U(I,J))
0066       21 CONTINUE
0067       11 CONTINUE
0068          IZ = 6
                CALL WLATCH(U,6,6,U)
0069          CALL EIGCC (U,6,1,EVEC,2,IZ,WR,IER)
0071          DO 5 I= 1,6
0072          DO 5 J=1,6
0073          ZZ(I,J) = CABS(Z(I,J))**2
0074        5 CONTINUE
0075        5 CONTINUE
0076            DO 420 I=1,6
0077            SUMZ(I)=0.
0078            DO 431 J=1,6
0079      431 SUMZ(I)=SUMZ(I)+ZZ(I,J)
0080      420 CONTINUE
0081            DO 432 I=1,6
0082            SNORM(I)=SQRT(SUMZ(I))
0083      432 CONTINUE
0084            DO 433 I=1,6
0085            DO 404 J=1,6
0086      404 Z(I,J)=Z(I,J)/SNORM(I)
0087      433 CONTINUE
0088            do j=1,6
0089            write(9,*)(z(i,j),i=1,6)
0090            end do
0091            DO 405 I=1,6
0092            DO 405 J=1,6
0093      406 ZZ(I,J)=CABS(Z(I,J))**2
0094      405 CONTINUE
C
0095          P(1) = PX
0096          P(2) = PY
0097          P(3) = PZ
```

```
0099          P(4) = PX
0100          P(5) = PY
0101          P(6) = PZ
0102          DO 10 J=1,5
0103          TOTP(J) = 0.
0104          DO 20 I=1,5
0105          CALP(I) = ZZ(I,J) * P(I)
0106          TOTP(J) = CALP(I) + TOTP(J)
0107       20 CONTINUE
0108       10 CONTINUE
0109          DO 30 J= 1,6
0110          TOTP(J) = .5 * TOTP(J)
0111       32 CONTINUE
0112          K(1) = KX
0113          K(2) = KY
0114          K(3) = KZ
0115          K(4) = KX
0116          K(5) = KY
0117          K(6) = KZ
0118          SQR = SQRT(1.2 + R)
0119          DO 50 J= 1,6
0120          TOTK(J,1)=0.
0121          DO 60 I = 1,3
0122          N = I+3
0123          CALK(I) = K(I) * (CABS(Z(I,J)*
              1(SQR/SQRT(2.2))+Z(N,J) *
              1((I-(0.0,1.0)*0)/(SQR*SQRT(2.0))))**2)
0124          TOTK(J,1) = CALK(I) + TOTK(J,1)
0125       60 CONTINUE
0126       50 CONTINUE
0127          DO 70 J=1,5
0128          TOTK(J,2) = 0.
0129          DO 80 I=1,3
0130          N = I+3
0131          CALK(I) = K(I) * (CABS(-Z(I,J)*
              1(I+(0.0,1.0)*0)/(SQRT(2.0)*SQR)
              1+ Z(N,J)*SQR/SQRT(2.0))**2)
0132          TOTK(J,2) = TOTK(J,2) + CALK(I)
0133       80 CONTINUE
0134       70 CONTINUE
0135          DO 90 I=1,6
0136          SUMK(I) = TOTK(I,1) + TOTK(I,2)
0137          DIFK(I) = TOTK(I,1) - TOTK(I,2)
0138       90 CONTINUE
      c
0139            do 1=1,5
0140            do j=1,6
0141            w(i,j) = 0.0
0142            end do
0143            end do
      c
0144          w(1,2) = WXY
0145          w(1,3) = WXZ
0146          w(2,3) = WYZ
0147          w(4,5) = WXY
0148          w(4,6) = WYZ
0149          w(5,6) = WYZ
```

```
0149            W(2,1) = WXY
0150            W(3,1) = WXZ
0151            W(3,2) = WYZ
0152            W(5,4) = WXY
0153            W(5,4) = WXZ
0154            W(5,5) = WYZ
      C
0155          DO 100 I=1,5
0156          M=I+1
0157          DO 100 J=M,5
0158          WIJ(I,J) = 0.
0159          DO 120 KK =1,3
0160          M=KK+3
0161          DO 120 L= 1,3
0162          M=L+3
0163          WIJ(I,J) = WIJ(I,J) +
             1    (CABS((CONJG(Z(KK,I)))*Z(L,J)
             1 + (CONJG(Z(M,I)))*Z(M,J)))**2 * W(KK,L)
0164      120 CONTINUE
0165      100 CONTINUE
0166          DO 152 I=1,6
0167      152 AIJ(I,I)=0.
0168          DO 140 I=1,5
0169          M=I+1
0170          DO 140 J=M,5
0171      140 WIJ(J,I) =  WIJ(I,J)
0172          DO 151 I=1,6
0173          DO 152 J=1,6
0174          AAA(I,J) = -AIJ(I,J)
0175      152 CONTINUE
0176      151 CONTINUE
0177          DO 153 I=1,6
0178          S(I) =0.
0179          DO 151 L=1,5
0180          S(I) = S(I)+AIJ(I,L)
0181      151 CONTINUE
0182      153 AAA(I,I) = SUME(I) + S(I)
0183          DO 91 I=1,6
0184          DO 92 J=1,6
0185          AA(I,J)=AAA(I,J)
0186       92 CONTINUE
0187       91 CONTINUE
0188          CALL LINV1F (AAA,6,6,WIJIN,4,WK1,IER1)
0189          CALL MULFF(WIJIN,TOTP,6,6,1,6,6,6,5,5,IER2)
0190          POL = 0.
0191          DO 300 J=1,5
0192          POL = POL +DIFF(J)*S(J)
0193      300 CONTINUE
      C
0194            return
0195          END
```

VARIABLES

Address	Type	Name	Address	Type	Name
2-000056D8	CHAR	AN1	2-000056D9	CHAR	AN2
5-00000004	R*4	AY	2-00005744	R*4	AYY
2-00005748	R*4	AZZ	2-000056F0	R*4	BETA
3-00000004	R*4	E	3-00000008	R*4	GAMA
2-000056FC	R*4	ZZZ	AP-00000000C0	R*4	H
2-00005720	R*4	HZ	2-00005750	I*4	I
2-00005778	I*4	IER2	2-00005758	I*4	IZ
4-00000000	R*4	KX	4-00000004	R*4	KY
2-00005770	I*4	M	2-00005764	I*4	MM
AP-00000010C0	R*4	POL	4-00000000	R*4	PX
2-00005710	R*4	Q	2-00005714	R*4	R
2-000056E0	C*8	SOR	2-00005760	R*4	T
2-00005730	R*4	TRCOS	2-0000573C	R*4	TRSIN
6-0000000P	R*4	WYZ	2-00005730	R*4	ZINU1
2-00005720	R*4	ZSY	2-00005724	R*4	ZUZ

Address	Type	Name	Address	Type	Name
5-00000000	R*4	AX	2-00005740	R*4	AXX
5-00000008	R*4	AZ	2-0000574C	R*4	AZY
2-00005700	R*4	CONV	3-00000000	R*4	D
2-000056F4	R*4	GIX	2-000056F8	R*4	GIY
2-00005718	R*4	HI	2-00005710	R*4	HY
2-0000575C	I*4	IER	2-00005774	I*4	IER1
2-00005754	I*4	J	2-00005768	I*4	KK
4-00000008	R*4	LZ	2-0000575C	I*4	L
2-00005750	I*4	N	AP-00000000B0	R*4	PHI
4-00000010	R*4	PY	4-00000010	R*4	PZ
2-00005708	R*4	RPHI	2-00005704	R*4	RTHETA
AP-00000000C0	R*4	THETA	2-00005734	R*4	TR
6-00000000	R*4	WXY	6-00000004	R*4	WXZ
2-00005618	C*8	ZINU2	2-00005728	R*4	ZGX

ARRAYS

Address	Type	Name	Bytes	Dimensions
2-00005390	R*4	AA	144	(6, 6)
2-00005420	R*4	AAA	144	(6, 5)
2-000052A0	R*4	CALK	24	(6)
2-000056C0	R*4	CALP	24	(6)
2-00005508	R*4	CALX	144	(5, 5)
2-00005288	R*4	DIFK	24	(5)
2-00000120	C*8	FFIC	48	(6)
2-00005378	R*4	J	24	(5)
2-00005480	R*4	K	24	(6)
2-000056A8	R*4	P	24	(6)
2-00005408	R*4	S	24	(5)
2-00005360	R*4	SNORM	24	(6)
2-00005270	R*4	SUMZ	24	(5)
2-00005348	R*4	SUMZ	24	(5)
2-00005240	R*4	TOTS	48	(6, 2)
2-00005558	R*4	TOTP	24	(5)
2-00000FF0	C*8	U	288	(6, 6)
2-00003FD0	C*8	UU	288	(6, 6)
2-00005470	R*4	V	144	(5, 5)
2-00005570	R*4	WIJ	144	(6, 6)
2-00005180	R*4	WIJIN	144	(6, 6)
2-00024210	R*4	WX1	4000	(1000)
2-00002150	C*8	WR	16000	(2000)
2-00000000	C*8	Z	288	(6, 6)
2-00005288	R*4	ZZ	144	(5, 5)

REFERENCES

01. H. Schuch, D. Stehlik, and K.H. Hausser, Z. Naturforsh. 26, 1944 (1971)

02. P. Lau, D. Stehlik, and K.H. Hauser, J. Mag. Res. 15, 270 (1974)

03. A. Pines, M.G. Gibby, and J.S. Waugh, J. Chem. Phys 59, 569 (1973)

04. M. Mehring, High Resolution NMR Spectroscopy in Solids, Chapt. 4 Springer-Verlag: Berlin (1976)

05. see e.g. C.P. Slichter, Principles of Magnetic Resonance, Chapt. 6 Springer-Verlag: Berlin (1978)
M. Goldman, Spin Temperature and Magnetic Resonance in Solids, Chapt. 2 Clarendon Press: Oxford (1970)

06. S.R. Hartman and E.L. Hahn, Phys. Rev. 128, 2042 (1962)

07. D.A. MacArthur, E.L. Hahn, and R.E. Walstedt, Phys. Rev. 188, 609 (1969)

08. A. Abragham, Principles of Nuclear Magnetism, Chapt. XII Oxford University Press: London (1961)

09. D. Stehlik, A Doehring, J.P. Colpa, E. Callaghan, and S. Kesmarky, Chem. Phys. 7, 165 (1975)
J.P. Colpa and D. Stehlik, Chem. Phys. 21, 273 (1977)
D. Stehlik and J.P. Colpa, Chem. Phys. 21, 289 (1977)
D. Stehlik, P. Rosch, P. Lau, H. Zimmerman, and K.H. Hausser, Chem. Phys. 21, 301 (1977)

10. D. Stehlik, "Mechanism of Optical Nuclear Polarization in Molecular Crystals" in Excited States, Vol. 3, ed. E.C. Lim,

Academic Press: New York (1975)

11. V. Macho, thesis, Free Univ. of Berlin (1981)

12. R. Furrer, M. Heinrich, D. Stehlik, and H. Zimmerman, Chem. Phys. 36, 27 (1979)

13. M. Tinkham, Group Theory and Quantum Mechanics, McGraw Hill: New York (1964)

14. J.H. van der Waals and M.S. de Groot, "Magnetic Interactions Related to Phosphorescence" in Triplet State, ed. A.B. Zahlan, Cambridge University Press: Cambridge (1967)

15. W.S. Veeman, thesis, Univ. of Leiden (1972)

16. W.S. Veeman, A.L.J. van der Poel and J.H. van der Waals, Mol. Phys. 29, 225 (1975)

17. S.J. Kohler, thesis, Univ. of California, Berkeley (1975)

18. J.D. Ellett, Jr., M.G. Gibby, U. Haebrlen, L.M. Huber, M. Mehring, A. Pines, and J.S. Waugh, in Adv. in Mag. Res., Vol. 3 (1971)

M.E. Stoll, A.J. Vega, an R.W. Vaughan, Rev. Sci. Instrum. 48, 800 (1977)

R.F.Karlicek, Jr., I.J. Lowe, J. Mag. Res. 32, 199 (1978)

19. V.R. Cross, R.K. Hester and J.S. Waugh, Rev. Sci. Instrum. 47, 1486 (1976)

20. E.O. Stejskal and J. Schaefer, J. Mag. Res. 14, 160 (1974)

21. W. Shih, thesis, Univ. of California, Berkeley (1979)

22. B. Leskovar, Nucl. Instr. and Meth. 47, 29 (1967)

23. J.G. Powles and P. Mansfield, Phys. Let. 2, 58 (1962)

J.G. Powles and J.H. Strange, Proc. Phys. Soc. 82, 6 (1963)

J.S. Waugh and C.H. Wang, Phys. Rev. 162, 209 (1967)

24. D.M. Burns and J. Iball, Proc. Roy. Soc. Lond. A 227, 200 (1955)

25. see, e.g. H.E. Buckley, Crystal Growth, John Wiley and Sons: New York, pg. 73 (1951)

26. H. Zimmerman, personal communication

27. M. Mehring, High Resolution NMR Spectroscopy in Solids, Chapt. 2 Springer-Verlag: Berlin (1976)

28. IMSL library, version 8.0, Houston, Texas (1980)

29. Oriel Corp. Catalog, Stamford, Conn.

30. D. Stehlik, private communication

31. K.H. Hausser, O. Lauer, H. Schuch, and D. Stehlik, Proc. XVIth Congress AMPERE, Bucharest (1970)

32. S. Pausak, A. Pines, and J.S. Waugh, J. Chem. Phys. 59, 591 (1973)

33. S. Pausak, J. Tegenfeldt, and J.S. Waugh, J. Chem. Phys. 61, 1338 (1974)

34. M. Mehring, High Resolution NMR Spectroscopy in Solids, Chapt. 5 Springer-Verlag: Berlin (1976)

35. J. van Dongen Torman and W.S. Veeman, J. Chem. Phys. 68, 3233 (1978)

36. W.S. Veeman, Phil. Trans. Roy. Soc. Lond. A 299, 629 (1981)

37. J. van Dongen Torman, W.S. Veeman, and E. De Boer, J. Mag. Res. 32, 49 (1978)

38. D.L. Van der Hart, J. Chem. Phys. 64, 830 (1976)

39. J.J. Chang, R.G. Griffin, and A. Pines, J. Chem. Phys., 62, 4923 (1975)

40. J. Tegenfeldt, H. Feucht, G. Ruschitzka, and U. Haeberlen, J. Mag. Res. 39, 509 (1980)

41. M. Gibby, thesis, M.I.T. (1972)

42. J.B. Stothers, Carbon-13 Spectroscopy, Academic Press: New York (1972)

43. see e.g. J.A. Pople, W.G. Schneider, and J.J. Bernstein, High Resolution NMR, McGraw Hill: New York (1959)

44. L.B. Schreiber and R.W. Vaughn, Chem. Phys. Let. 26, 586 (1974)

45. K.S. Krishnan, and Banerjee, Philos. Trans. Roy. Soc. Lond. 234, 265 (1935)

46. J.A. Osborn, Phys. Rev. 67, 351 (1945)

47. D. Stehlik, personal communication

personal observation

48. J. Giraud and C. Marzin, Org. Mag. Res. 12, 647 (1979)

L.F. Johnson and W.C. Jankowski, ^{13}C NMR Spectra, Wiley: New York (1972)

Additional references (in chronological order)

ONP

J.P. Colpa, K.H. Hausser, and D. Stehlik, Z. Naturforsch. 26a, 1792 (1971)

G.Dittrich, D. Stehlik, and K.H. Hausser, Z. Naturforsch. 32a, 652 (1977)

J.P. Colpa, F Seiff, and D. Stehlik, Chem. Phys. 33, 79 (1978)

H.M. Vieth, V. Macho, and D. Stehlik, Chem. Phys. Let. 60, 368 (1979)

H.M. Vieth, V. Macho, and D. Stehlik, J. Phys. Chem. 83, 3435 (1979)

D. Stehlik, R. Furrer, and V. Macho, J. Phys. Chem. 83, 3440 (1979)

J.P. Colpa, D. Stehlik, and H.M. Vieth, Chem. Phys. 47, 73 (1980)

EPR

R. Furrer, J. Gromer, A. Kacher, M. Schorer, and H.C. Wolf, Chem. Phys. 9, 445 (1975)

R. Furrer, J. Petersen, and D. Stehlik, Chem. Phys. 44, 1 (1979)

V. Macho, J.P. Colpa, and D. Stehlik, Chem. Phys. 44, 113 (1979)

R. Furrer, F. Fujara, and J. Petersen, J. Chem. Phys. 73, 3139 (1980)